Folkhälsan Institute of Genetics,
and
Neuroscience Center and
Research Programs Unit, Molecular Neurology, University of Helsinki,
and
Graduate School of Brain and Mind

IMAGING STUDIES IN THE MOUSE MODEL OF PROGRESSIVE MYOCLONUS EPILEPSY OF UNVERRICHT-LUNDBORG TYPE, EPM1

Otto Manninen

ACADEMIC DISSERTATION

To be presented for public examination with the permission of the Faculty of Medicine of the University of Helsinki in the Biomedicum Helsinki, Lecture Hall 3, Haartmaninkatu 8, Helsinki on Friday, October 16th 2015, at 12 noon.

Helsinki 2015

Dissertationes Scholae Doctoralis Ad Sanitatem Investigandam
Universitatis Helsinkiensis 75/2015

ISBN 978-951-51-1522-5 (paperback)
Hansaprint Oy

ISBN 978-951-51-1523-2 (PDF)
Helsinki 2015

http://ethesis.helsinki.fi

Supervised by

Professor Anna-Elina Lehesjoki, MD PhD
Folkhälsan Institute of Genetics
Research Programs Unit, Molecular Neurology and Neuroscience Center;
University of Helsinki
Helsinki, Finland

Adjunct Professor Outi Kopra, PhD (Deceased)
Folkhälsan Institute of Genetics
Research Programs Unit, Molecular Neurology and Neuroscience Center;
University of Helsinki
Helsinki, Finland

Reviewed by

Professor Heikki Tanila, MD PhD
A.I.Virtanen Institute for Molecular Sciences, University of Eastern Finland,
Department of Molecular Neurobiology, Kuopio, Finland

Docent Timo Kurki, MD PhD
Department of Radiology, Turku University hospital, Turku, Finland

Thesis advisory committee

Professor Heikki Tanila, MD PhD
A.I.Virtanen Institute for Molecular Sciences, University of Eastern Finland,
Department of Molecular Neurobiology, Kuopio, Finland

Adjunct Professor Jaana Vesterinen, PhD
Institute of Biomedicine, Biochemistry and Developmental Biology,
University of Helsinki
Helsinki, Finland

Opponent

Professor Taina Autti, MD PhD
Department of Radiology, Medical Imaging Center, Helsinki University Central Hospital,
Helsinki, Finland

Custos

Professor Päivi Peltomäki, MD PhD
Department of Medical Genetics, University of Helsinki
Helsinki, Finland

Dedicated to Outi.

'I have not failed. I've just found 10,000 ways that won't work.'

- Thomas Edison-

TABLE OF CONTENTS

LIST OF ORIGINAL PUBLICATIONS

I : **Manninen O**, Laitinen T, Lehtimäki K, Tegelberg S, Kopra O, Lehesjoki A-E, Gröhn O, Kopra O: Progressive Volume Loss and White Matter Degeneration in Cstb-deficient Mice: a Diffusion Tensor and Longitudinal Volumetry MRI Study. PLoS One. 2014 DOI: 10.1371/journal.pone.0090709

II : **Manninen O**, Koskenkorva P, Lehtimäki K, Kopra O, Kälviäinen R, Gröhn O, Lehesjoki A-E, Vanninen R: White matter degeneration with Unverricht-Lundborg progressive myoclonus epilepsy: a translational diffusion-tensor imaging study in patients and cystatin B-deficient mice. Radiology. 2013;269:232-9

III: **Manninen O**, Puolakkainen, T, Lehto J, Harittu E, Kallonen A, Peura M, Laitala-Leinonen T, Kopra O, Kiviranta R, Lehesjoki A-E: Impaired osteoclast homeostasis in the cystatin B -deficient mouse model of progressive myoclonus epilepsy EPM1. Under revision Bone Reports 2015

Author's contribution:

I: Author conducted all the experiments, analysis and image preparation, and participated in the study design and manuscript preparation.

II: This study was carried out in a translational setting together with another research group studying EPM1 patients. Author conducted all the animal experiments, as well the analysis of the data and participated in the study design and manuscript preparation. As the patient data has been extensively addressed in thesis of Päivi Koskenkorva (2012), only animal experiments are described in thesis, however the implications of the patient findings are discussed in this thesis.

III: Author conducted all the uCT and cell culture experiments, as well as data analysis and image preparation, and participated in the study design and manuscript preparation.

The publications are referred to in the text by their Roman numerals, and included at the end of the thesis. Unpublished data are also presented. The original articles are reproduced with the permission of the respective copyright holders.

ABBREVIATIONS

List of the abbreviations that appear more than once and in more than one section are presented here.

a-MEM = alpha modification of Eagle's medium

AD = axial diffusion

ANOVA = analysis of variance

BMP = bone morphogenic proteins

BSA = bovine serum albumin

Cat K = cathepsin K

CNS = central nervous system

CSTB = cystatin B

Cstb$^{-/-}$ mouse = *Cstb* gene knockout mouse model of EPM1

DAB = diaminobenzidine tetrahydrochloride

DTI = diffusion tensor imaging

DWI = diffusion weighted imaging

EEG = electroencephalogram

EPM1 = progressive myoclonous epilepsy type 1; Unverricht-Lundborg disease

FA = fractional anisotropy

FACS = fluorescence activated cell sorting

FOV = field of view

fMRI = functional magnetic resonance imaging

JME = juvenile my oclonic epilepsy

M-CSF = macrophage colony stimulating factor

MBP = myelin basic protein

MD = mean diffusivity

MMP9 = matrix metallopeptidase 9

MRI = magnetic resonance imaging

MRS = magnetic resonance spectroscopy

MS = multiple sclerosis

NMR = nuclear magnetic resonance

NT = echo train length

PBS = phosphate-buffered saline

PME = progressive myoclonous epilepsy

RANKL = receptor activator of nuclear factor kappa-B ligand

RD = radial diffusion

ROI = region of interest

TBSS = tract-based spatial statistics

TE = echo time

TEM = transmission electron microscopy

TFCE = threshold free cluster enhancement

TMS = transcranial magnetic stimulation

TR = repetition time

TRACP 5b = tartrate-resistant acid phosphatase 5b

TRAP-kit = leukocyte acid phosphatase kit

VBM = voxel-based morphometry

WM = white matter

μCT = microtomography

ABSTRACT

Unverricht-Lundborg type progressive myoclonus epilepsy (EPM1, OMIM 254800) is an autosomal recessive disorder characterized by onset at the age of 6 to 16 years, incapacitating stimulus-sensitive myoclonus and tonic-clonic epileptic seizures. It is caused by mutations in the gene encoding cystatin B (*CSTB*). However, the disease processes leading to the observed symptoms are currently unclear. Clinical magnetic resonance imaging (MRI) of the brain has shown neurodegenerative changes and computed tomography data have suggested a bone phenotype. This thesis examined the disease processes and the background of the pathological changes in the brain and the bone, utilizing modern imaging methods and image analysis methodology complemented with experimental data in the mouse model (the *Cstb*$^{-/-}$ mouse) of the disease.

In order to gain a comprehensive picture of the disease progression in the brain, we performed a longitudinal imaging study in the *Cstb*$^{-/-}$ mouse. Animals were studied from the pre-symptomatic to fully symptomatic disease stages (1-6 mo). For studying atrophic changes, *in vivo* MRI volumetry was preformed once a month from 1 to 6 months of age. For investigating white matter (WM) changes, *ex vivo* diffusion tensor imaging (DTI) was performed at 2, 4 and 6 months. The fractional anisotropy (FA) maps derived from DTI data were analysed using track based spatial statistics (TBSS) that provided us with a hypothesis-free analysis of white matter changes. *In vivo* volumetry showed progressive volume loss in *Cstb*$^{-/-}$ mice over time, the rate of which was neither spatially nor temporally uniform over the brain. TBSS revealed progressing FA decrease, suggesting severe and widespread WM damage, with most drastic changes in the cerebellum and the thalamus.

Subsequently the congruence of the observed WM changes between the mouse model and EPM1 patients were evaluated. *In vivo* DTI data from fully symptomatic adult patients and *ex vivo* data from fully symptomatic (6 mo) *Cstb*$^{-/-}$ mice were analysed using TBSS with matching protocols. The results revealed extensive changes with a pattern of chronic WM degeneration in EPM1 patients, with similar alterations detected in *Cstb*$^{-/-}$ mice. Furthermore, previously unknown brain regions were shown to be affected both in patients and in mice. The imaging data were then used to guide tissue level analyses in mice. The microstructural counterpart of the areas with decreased FA in mice was characterized by immunohistochemistry and transmission electron microscopy. Based on the tissue level findings, the extensive changes identified by DTI in both EPM1 patients and in *Cstb*$^{-/-}$ mice are probably a consequence of widespread WM loss upon axonal degeneration, and likely contribute to the motor disturbances present in the disease.

Finally, we characterized the bone changes underlying the observed skeletal phenotype in EPM1 patients by performing microtomography (μCT), histology, and *in vitro* cell culture experiments with the *Cstb*$^{-/-}$ mouse. Analysis of bone microstructure in *Cstb*$^{-/-}$ mice using μCT revealed structural changes. Moreover, histology confirmed both structural and functional alterations. The basis of these findings was investigated by studying the functionality of bone resorbing osteoclasts differentiated *in vitro* from bone marrow. In resorption pit formation assays, less and smaller resorption pits were formed by *Cstb*$^{-/-}$ osteoclasts, indicating decreased resorptive capacity, likely due to a decrease in osteoclast numbers. These data imply that the skeletal changes in *Cstb*$^{-/-}$ mice and EPM1 patients are a result of CSTB deficiency leading to altered osteoclast function, and the results would indicate that *CSTB* has a more substantial role as a modulator of bone metabolism than previously thought.

Our results showed high correlations of the atrophy, WM and bone phenotypes between EPM1 patients and *Cstb*$^{-/-}$ mice and provided information about brain and tissue level changes present in these pathologies. High correlation between the mouse model and the findings in patients provided further affirmation for the use of the mouse model in EPM1 research. Furthermore, the results provided new insight both into the progression of brain pathology and the processes underlying the bone changes present in the disease. Finally, our research introduced new methodologies for research in mouse models of neurodegenerative diseases, and raised the prospects of future research.

TIIVISTELMÄ

Etenevä myoklonusepilepsia (Unverricht-Lundborgin tauti, EPM1) on suomalaiseen tautiperimään kuuluva, autosomaalisesti peittyvästi periytyvä sairaus, jonka ensimmäiset oireet havaitaan 6–15 vuoden iässä. Ensimmäiset oireet ovat useimmiten ulkoisten ärsykkeiden laukaisemia lihasnykäyksiä tai epileptisiä kohtauksia. EPM1 aiheutuu virheistä kystatiini B (CSTB)-proteiinia koodaavassa geenissä ja vaikka taudin aiheuttava geenivirhe on selvitetty, oireisiin johtavat tautimekanismit ovat edelleen tuntemattomat. Kliininen magneettikuvantaminen on osoittanut potilaiden aivoissa harmaan aineen vauriota ja tilavuudenalenemaa ja tietokonekerroskuvauksessa potilailla on havaittu kallon luiden paksuuntumista. Tässä väitöskirjatyössä pyrittiin kartoittamaan EPM1:n etenemistä ja havaittujen muutosten aikaansaavia kudos- ja solutason muutoksia käyttäen moderneja kuvantamis- ja kuvankäsittelymenetelmiä sekä histologiaa ja soluviljelykokeita taudin kystatiini B puutteisessa (*Cstb*$^{-/-}$ hiiri) hiirimallissa.

Taudin etenemistä aivoissa selvitettiin suorittamalla pitkittäisseurantaa taudin hiirimallissa. Kuvantaminen aloitettiin oireettomissa hiirissä, ja seurantaa jatkettiin kaikkien taudinkuvaan kuuluvien oireiden ilmenemiseen asti (1–6 kk). EPM1:ssä esiintyvän tilavuudenaleneman etenemistä tutkittiin *in vivo* magneettikuvantamisella, ja valkean aineen muutoksia *ex vivo* diffuusiotensorikuvamisella. Käyttäen hypoteesivapaata vokselipohjaista analyysimenetelmää (Track based spatial statistic, TBSS) valkean aineen muutoksia seurattiin analysoimalla fraktionaalisen anisotrofian (FA) muutoksia. Havaitsimme *Cstb*$^{-/-}$ hiirissä etenevän tilavuudenaleneman, jonka määrä vaihteli eri aivoalueiden välillä. Diffuusiotensorikuvantaminen osoitti etenevään aivokudoksen vaurioon viittaavan FA aleneman, joka ilmeni voimakkaimmin talamuksissa ja pikkuaivossa.

Seuraavaksi kartoittamme havaittujen valkean aineen vaurioiden yhtenevyyttä hiirimallissa ja potilaissa. Aikuisten EPM1 potilaiden *in vivo* ja aikuisten *Cstb*$^{-/-}$(6kk) hiirten *ex vivo* diffuusiotensorikuvantamisdata analysoitiin käyttäen identtisiä TBSS-protokollia. Tulokset osoittivat laaja-alaisia, krooniseen rappeumaan viittaavia valkean aineen muutoksia EPM1-potilaissa, ja hiirimallissa havaittiin vastaavat muutokset. Analyysi paljasti sekä potilaissa, että *Cstb*$^{-/-}$ hiirissä muutoksia aivoalueilla, joiden ei ole aikaisemmin tiedetty EPM1:ssä vaurioituneen. Havaittujen muutosten alkuperää tutkittiin *Cstb*$^{-/-}$ hiirissä kudostason tarkastelulla soluleikkeistä immunohistokemiallisin värjäyksin, ja elektronimikroskooppisella analyysillä. Tulokset osoittivat että sekä EPM1 potilaissa että hiirimallissa diffuusiokuvantamisella havaitut valkean aineen muutokset ovat seurausta aksonikadosta, ja ovat todennäköisesti yhteydessä taudissa esiintyviin liikehäiriöihin.

EPM1-potilailla havaittujen luumuutosten taustoja selvitettiin *Cstb* $^{-/-}$ hiirissä tietokonekerrokuvauksella (microtomography; μCT), kudosleikevärjäyksillä ja soluviljelykokein. Tietokonekerroskuvaus osoitti luun hienorakenteen muuttuneen *Cstb* $^{-/-}$ hiirissä, minkä lisäksi kudosleikevärjäyksissä todettiin luussa sekä rakenteellisia että toiminnallisia muutoksia. Näiden muutosten alkuperää kartoitettiin luuta kierrättävien osteoklastien soluviljelykokein. Kun solujen kykyä hajottaa luuta tutkittiin, havaittiin *Cstb* $^{-/-}$ hiirten osteoklastien muodostavan vähemmän ja pienempiä resorptiivisia kuoppia. Tämä kertoo osteoklastien heikommasta hajotuskyvystä, ja muutos *Cstb* $^{-/-}$ hiirissä on todennäköisesti seurausta matalammasta solumäärästä viljelmissä. Vaikuttaa siltä, että sekä EPM1 potilaissa, että taudin hiirimallissa havaitut luumuutokset ovat seurasta kystatiini B puutteen aiheuttamista muutoksista osteoklastien toiminnassa. Nämä tulokset viittaavat siihen, että kystatiini B:llä on aikaisempaa suurempi rooli luun metabolian säätelyssä.

Tutkimustuloksemme hiirissä vastasivat potilaissa havaittua aivojen tilavuudenalenemaa, valkean aineen vaurioita ja luulöydöksiä, ja pystyimme osoittamaan niihin johtavat kudos- ja solutason muutokset. Havaintomme valottavat EPM1:n huonosti tunnettua etenevää taudinkuvaa, sekä ennestään tunnettujen muutosten taustaa, ja löydösten yhteneväisyys hiirimallissa ja potilaissa rohkaisee EPM1-tutkimuksen jatkamista *Cstb* $^{-/-}$ hiirimallissa. Väitöskirjatutkimus esitteli myös uusia menetelmiä aivorappeumatautien hiirimallitutkimuksessa sekä avasi uusia tutkimusalueita EPM1:n taudinkuvan selvittämisessä.

1 INTRODUCTION

"En usko ennen kuin näen."

Old Finnish proverb

We perceive the world around us predominantly through our vision, and as the above proverb states, things are often believed only after they have been seen. For observing things too far away to see with the naked eye, we use binoculars or even telescopes. For things that are too small to see otherwise, we use magnifying glasses or microscopes. Events or details that would not otherwise be observable can be witnessed with the aid of different imaging methods. Occurrences too fast to perceive as they happen can be visualised in slow motion, and extremely slow changes become clear in time-lapse. Similarly, thermography cameras visualises differences in temperatures and x-ray imaging allows us to see through and inside things.

In observational sciences, such as astronomy, observing the surroundings gives the scientist an opportunity to gain information on what has happened or is happening, however the researcher does not interact with or manipulate the events. In experimental research the scientific method is utilized for acquiring new knowledge. Based on previous knowledge and reasoning, a hypothesis is formulated and experiments testing the hypothesis are conducted. Once the outcome of the experiment is observed, results can be analysed and based on the results, a hypothesis is confirmed or re-evaluated. In experimental sciences, observing the outcome of the experiment is commonly observed visually. Combined with the scientific method, our yearning for visual proof constantly transforms the worldview by delivering new insight into the universe and its inner workings. In this thesis, modern imaging methods were combined with the experimental hypotheses and the approach was able to provide new insights into previously unknown pathological processes in a disease.

REVIEW OF THE LITERATURE

1.1 MACRO- AND MICROANATOMICAL BASIS OF THE STUDY SUBJECT

1.1.2 Cellular organisation of the brain

"I am a brain, Watson. The rest of me is a mere appendix."

Arthur Conan Doyle, Sherlock Holmes - The Adventure of the Mazarin Stone

Due to its paramount function and structural complexity, the organisation of the mammalian brain has been extensively studied (Cowan, Harter & Kandel 2000). The neuronal doctrine, or the theory that the nervous system consists of individual interconnected cells, neurons, is considered the groundwork for modern neuroscience. It was first described by Santiago Ramón y Cajal (Llinas 2003), and for this groundbreaking discovery he was awarded the Nobel Prize in medicine (Nobel Lectures Physiology or Medicine 1901–1921). The following description of the composition and basic organisation of the brain (**Figure 1**) has been adapted from a description given by Purves et al (Purves 2012). The basic building block of the central nervous system (CNS) is a neuron, an excitable cell that is highly specialized in the transmission and processing of signals through electric and chemical means. Multiple neurons connect to each other to form neuronal networks that transmit signals in the brain. While there are multiple neuron types that vary in structure and function, their basic organisation is the same. Neurons consist of a main body called the soma, extensions of the soma called dendrites that receive signals into the neuron, and axons, cable like projections to that transmit signals to other neurons through synapses. The signal transmission in axons happens through small electric signals generated through changes in cell membrane potential along the axons. As the axons project over long distances, the insulating myelin sheath surrounding the axon ensures fast and efficient signal transduction. Neurons connect to each other through synapses, special neuron-to-neuron connections that allow transmission of signals from one cell to another. The signal transmission from one cell to another usually happens through the synaptic cleft with the aid of neurotransmitters, signal transmission molecules stored in synaptic vesicles in the axon side of the synapse. These neurotransmitters are released into the synaptic cleft from the pre-synaptic side, and bind to receptors on the postsynaptic side. In some cases signal transmission occurs directly through electric signalling from cell to cell.

A gross histological division between brain regions predominantly containing cell bodies of neurons or axons into respective grey and white matter is commonly used. The axon-dense part of the brain tissue, that is rich in myelinated axons and oligodendroglia, is called white matter, due to the historical fact that formalin fixed tissue has a light, almost white appearance as a result of its high myelin content. Regions that contain predominantly neuropil, meaning soma, dendrites, astroglia, microglia and unmyelinated axons, are referred to as grey matter. This is due to the noticeably darker appearance in formalin fixed brain tissue. The function of the white matter is to relay signals between different regions of brain, where they are processed in the neurons located in the grey matter. Due to the communicative function of the white matter, deterioration in its functional integrity has drastic consequences. In for instance multiple sclerosis (MS) (Mallucci et al. 2015, Criste, Trapp & Dutta 2014) and leukodystrophy (Groeschel et al. 2012), demyelination is known to produce a wide range of motor, sensory and psychiatric symptoms.

While neurons have historically been considered the predominant cell type in the brain, they are aided in their task to a great degree by the neuroglial cells. The glia do not directly take part in signal transmission, but rather have a supportive function. The glial cells were primarily considered a to be an unimportant filler or merely structural cells in the brain, hence the Greek name meaning 'glue' (Baumann, Pham-Dinh 2001). While more and more the tasks of the glial cells are still discovered, they currently are known to play important roles in aiding neurons in the formation and maintenance of neuronal circuits, and they have been identified to play a role in insulating axons, maintaining the ionic balance of the extracellular space and supporting synaptic transmission (Allen, Barres 2009). Oligodendroglial cells are responsible for ensheathing axons in layers of myelin, and maintaining these layers to ensure efficient signal transduction. Astroglia get the their name from their star like shape, and function to provide regulation of the extracellular space by removing excess ions and recycling neurotransmitters, and thus maintaining an environment suitable for the transmission of signals. Microglia, a specific type of glial cell, are the resident immune response unit in the CNS that scan the brain for injury or infection and remove pathogens, dead cells and debris via phagocytosis. While activation of microglia is observed in most neuropathological conditions, the role of microglia in the disease processes of CNS disorders is still debated (Prinz, Mildner 2011, Allen, Barres 2009).

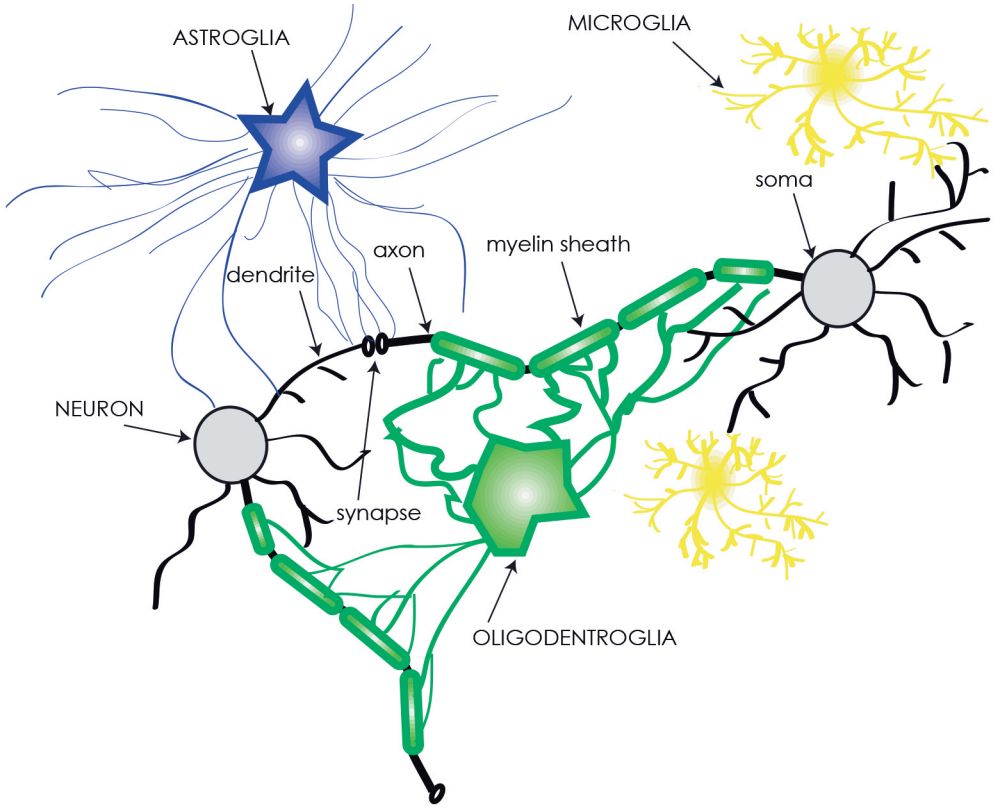

Figure 1. Central cell types in the nervous system. The diagram illustrates central celltypes in the brain and their interactions. Shown are astroglia (purple), neurons (grey), microglia (yellow) and oligodentroglia (green). Different parts of the neuron have also been marked in the image.

The described fundamental cellular configuration forms the functional circuitry of the brain, with individual structures forming distinguishable functional and anatomical units with dedicated tasks. The layout and the function of the brain regions most relevant to the subject matter of this thesis, the thalamocortical system and the cerebellum, is reviewed in detail in following chapters.

1.1.3 Thalamocortical system

The thalamic nuclei are responsible for conveying signals between different subcortical areas and the cortex, and this signal relay consisting of the cerebral cortices, the thalamus and their connecting fibres is referred to as the thalamocortical system or the thalamocortical relay. The cortices are responsible for the higher cognitive tasks and have dedicated motor, sensory and cognitive areas with distinct functions located in their respective areas. The sensory information is received by the primary

sensory cortical areas and the output of the primary motor cortex is to the spinal cord while the higher order sensory and motor areas integrate and process information. All the different regions, however, share a six-layered (referred to as layers I–VI) organisation. Each layer consists of its own characteristic cell types, function and connections with distinct contribution to the neuronal processing. Layer I consists mainly of laterally linked axons that connect different cortical regions, while layers II and III are mostly responsible for output over different cortical areas. The neurons in layer IV receive input from the thalamus and are responsible for distributing it to other cortical layers. Finally, layers V and VI receive information from the cortex and relay it to the thalamus, basal ganglia, brain stem and spinal cord.

The thalamus has a paramount impact in the cortical processes as a hub that most of the cortical information travels through. It is situated between the cerebellum and the midbrain, and it is composed of individual nuclei that are connected to their respective cortical regions. The information received by thalamic nuclei from sensory pathways and subcortical regions (and from layer V from cortical regions excluding the originating relay site) is conveyed to cortical layer IV, where it is spread to other layers. The corticothalamic fibres running from layer V provide afferent projections from the cortex to the thalamus, and some modulatory signals are also received from layer VI (**Figure 2**). While the thalamo-cortico-thalamic circuit is incompletely understood, it is known have a synchronising function, a filtering task to the cortical inputs and integrating information, as well as an executive role of timing and relaying cortical output. Besides the relay function, the thalamus is also thought to contribute to processing of sensory information and is known to have a role in verbal, motor and sensory memory (Purves 2012). A recent review concluded that the thalamococortical and corticothalamic networks that participate in governing sleep and consciousness contribute to the observed alterations in the state of consciousness in absence epilepsies (Bagshaw et al. 2014) and a voxel based morphometry (VBM) study in juvenile myoclonic epilepsy and idiopatic generalized epilepsy patients reported decreased functional thalamocortical connectivity contributing to the symptoms (Kim et al. 2014). Clinical studies have also demonstrated that thalamic lesions lead to ataxia (Solomon et al. 1994, Melo et al. 1992) and an imaging study investigating deep brain stimulation also showed involvement of the cerebello-thalamo-cortical network in the control of tremor and myoclonic tremor (Coenen et al. 2014).

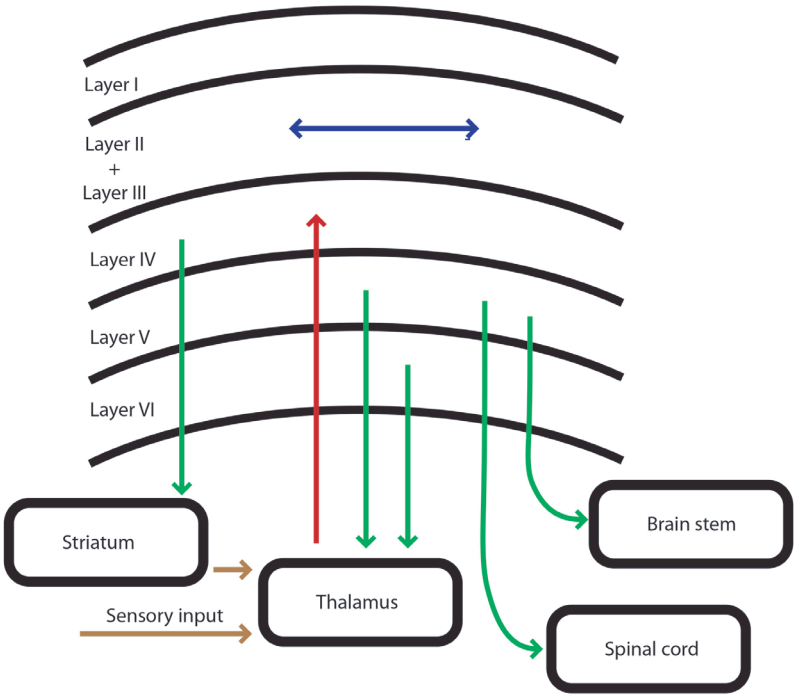

Figure 2. Simplified diagram of thalamocortical connectivity. The diagram illustrates corticothalamic, thalamocortical and corticocortical connectivity with arrows illustrating signalling directions. The layered structure of the cortex is also illustrated.

1.1.4 Cerebellum

The cerebellum is located at the base of the skull and consists of gyri: folded layers of cortex, covering white matter that surround a grey matter structure called deep cerebellar nuclei (**Figure 3)**. Due to it's small size and appearance that parallels the cereberal cortices, the Latin 'cerebellum' translates as 'little brain' (Butts, Green & Wingate 2014). While the cerebellum is known have a role in cognitive functions, language, attention and regulating fear responses, its most important tasks are in motor control (Wolf, Rapoport & Schweizer 2009). The cerebellum itself does not govern movement, but it ensures that various motor systems act in unison to produce intended action by providing accuracy, timing and coordination to movements that require a high degree of synchronization.

The layout of the cerebellum is highly symmetrical with 10 lobules, with each lobule consisting of a matching set of neuronal elements with a laminated cerebellar cortex, and grey matter structures called central deep cerebellar nuclei that are located at the centre of the cerebellar white matter. The deep cerebellar nuclei are hubs of cerebellar information transfer and almost all output fibres from the cerebellum

originate from there. The deep cerebellar nuclei receive excitatory input from mossy fibres and climbing fibre pathways and inhibitory input from Purkinje cells. On a larger scale, the cerebral cortex receives information from the cerebellum through the thalamus, and sends it to the cerebellum via the pons. The aim of this system is to detect discrepancies between planned action, and actual performed movements, and rectify motor errors. While errors in movement are corrected in real time, these corrections are also stored and form the foundation of motor learning (Purves 2012) and according to a review by Fine, Ionita and Lohr, the cerebellum to also has a role in cognitive functions such as verbal fluency, abstract reasoning, planning, intonation of speech and the correct use of grammar (Fine, Ionita & Lohr 2002). Furthermore, a recent review also concluded cerebellum to have a role in emotional processing in fear and motor responses to emotion (Strata 2015), and speech and non-motor language function (Marien et al. 2014).

As the cerebellum itself does not initiate or govern movement, the disorders of the cerebellar function do not as such manifest as absence or excess of movement and are instead commonly observed as deficits in the management of motor function. In a patient with a focal thalamic lesion, the role of cortico-cerebellar interactions in motor error prediction was demonstrated by investigating impairment in adaptive eye saccades (Zimmermann et al. 2015)and in a study investigating psychomotor function in patients with cerebellar lesions, inadequate hand-eye coordination highlighted the corrective role of the cerebellum in producing intended movement, as well as a cerebellar role in visual function (Sailer, Eggert & Straube 2005). A diffusion weighted imaging (DWI) study of traumatic brain injury patients demonstrated a decrease in cerebellar functional connectivity that corresponded with inadequate balance and postural control (Drijkoningen et al. 2014). A VBM study coined progressing cerebellar atrophy with deteriorating motor function in spinocerebellar ataxia (Mascalchi et al. 2014) and a functional magnetic resonance imaging (fMRI) study with a rhythmic the finger-tapping task in patients with tremor demonstrated alterations in cerebellar motor output (Buijink et al. 2015), illustrating the cerebellar role in limiting undesired movement and the impairments in motor performance that manifest when this task is incompetently performed.

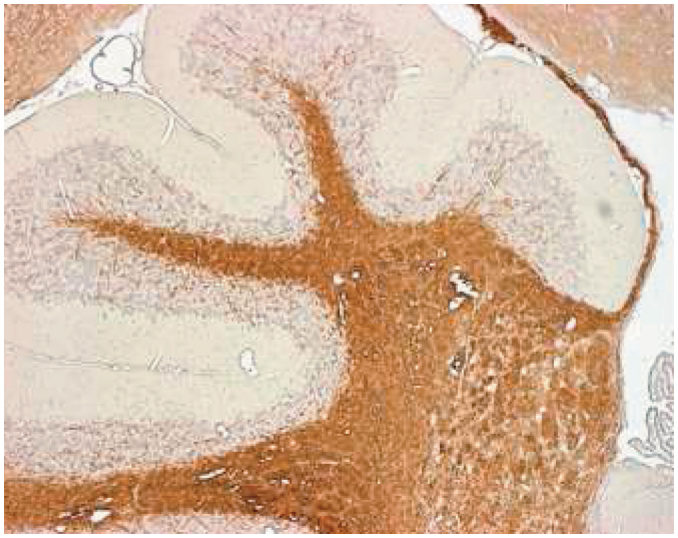

Figure 3. Immunohistogical staining of mouse cerebellum. Immunohistological staining against myelin proteolopid protein (brown colour) in a sagittal cerebellar tissue section illustrates the white matter under the gyrous cortical surface of the cerebellum.

1.1.5 Principles of bone remodelling

All vertebrates have an endoskeleton, commonly referred to as the skeleton, that offers protection and support for the internal organs, and enables locomotion for the organism by providing support and leverage as well points of contact for muscles. This skeleton consists of various types of connective tissue: ligament, tendon, cartilage, and most importantly, bone. The following description of bone, and it's remodelling has been adapted from a book by Currey (Currey 2013).

Bone is seen in a multitude of shapes and sizes, and bone tissue consists two distinct bone types, stiff and tough cortical bone and light and porous trabecular bone. The cortical bone forms the hard exterior of the bones, while the inside consists of light and porous trabecular bone which provides support and helps distribute the forces subjected to the cortical bone. While these two components differ in microstructure and mechanical properties, they share the same principal arrangement. Bone is structurally a composite of two major components. The mineral calcium phosphate provides mechanical strength and stiffness to the bone, and the organic collagen matrix supports the structure and provides elasticity and fracture resistance to the tissue. Bones are also known act as reserve for calsium, and trabecular bone contains bone marrow, which is responsible for haematopoiesis.

Due to its role of in locomotion, bone is constantly under mechanical stress and requires maintenance and repair, as well as remodelling. This is a dynamic process,

in which old bone is digested and new bone formed. Bone is digested by osteoclasts, multinucleated cells rich in lysosomes. They are of monocyte origin and are formed through fusion of pre-osteoclasts. The osteoclasts attach to surface of the bone and form a sealing zone at the periphery of the cell, which creates a lumen between the osteoclast and the bone into which the bone digesting enzymes are secreted to. Osteoclasts digest the bone by breaking down the collagen matrix with collagenases, most prominently cathepsin K (Cat K) and dissolving the mineral component of the bone. Bone is synthesised by cells at the surface of the bone called osteoblasts. The formation of new bone happens in a two stages. First, the osteoblasts secrete the organic component of the bone matrix, called osteoid, consisting predominantly of collagen I. Following this the osteoid is mineralised with help of alkaline phosphatases, creating mineralized bone. Osteoblasts that are no longer at the surface of the bone, become incorporated in the bone and turn into osteocytes, cells responsible of maintaining bone homeostasis. Disturbances in the homeostasis of the bone formation and resorption lead to pathologic changes in bone composition, such as osteopetrosis (Boyce et al. 2014), or osteoporosis (McGowan et al. 2014)

1.2 PROGRESSIVE MYOCLONUS EPILEPSY, EPM1

"People think that epilepsy is divine simply because they don't have any idea what causes epilepsy. But I believe that someday we will understand what causes epilepsy, and at that moment, we will cease to believe that it's divine. And so it is with everything in the universe."

-Hippocrates-

The brain is mechanically shielded from external insults by the skull, and meninges, as well as cushioned by the cerebrospinal fluid. It is also biologically protected by the blood-brain barrier and the immune system. Still, owing to the extreme complexity of the brain and the delicate biological balance needed to maintain its normal function, very small changes, such as defective function of a single cell type or lack of a single protein, can disrupt its equilibrium.

One of the most devastating neurological disorders is epilepsy, a group of neurological disorders characterised by a common symptom of epileptic seizures that can vary in type, severity, length, rate of reoccurrence, origin and cause (Berg et al. 2010, Purves 2012). The seizures are a result of abnormal and excessive neuronal activity in the brain following genetic, metabolic or structural changes in the brain and different epilepsy types vary in type and cause of seizures. The presentation of the seizure types varies, ranging from partial to generalized, and seizures can have motor, sensory and psychological manifestations (Berg et al. 2010). A variety of

causes for epilepsy are known, and the classification relies on the causative factors, with a division between acquired epilepsies and epilepsies with a genetic cause **(Table 1)** (Shorvon 2011). Tumours, traumatic brain injury, stroke or infections are a few examples of the numerous structural and metabolic changes in the brain known to cause epilepsies (Berg et al. 2010). Genetic causes for epilepsies vary from monogenic changes, to disorders known to result from multi-gene predisposition that environmental factors may also contribute to (Noebels 2015). Progressive myoclonic epilepsies (PME) are a group of rare epilepsy syndromes that are caused by a range of genetic defects (Berkovic, So & Andermann 1991). In PMEs, such as Lafora disease or Batten disease, an identified genetic cause translates into a lack or deficiency in protein expression, which in turn causes neurodegeneration that manifests as epileptic seizures, among other symptoms and pathologies (Minassian 2014). An identified genetic defect that translates into epilepsy through neurodegeneration also underlies a PME type called progressive myoclonic epilepsy type 1 (EPM1), the pathological processes of which this thesis investigates (Pennacchio et al. 1996) **(Table1)**.

In 1891, Heinrich Unverricht described a syndrome of progressive myoclonus epilepsy in patients of Baltic origin (Unverricht 1891, Unverricht 1895) and Herman Bernhard Lundborg reported the hereditary pattern of the similar syndrome in a Swedish family at the turn of the century (Lundborg 1912, Lundborg 1903). Based on the Baltic origin of the patients, the disease was first known as Baltic epilepsy, or Baltic myoclonic epilepsy, with a similar syndrome with patients from Mediterranean countries known as Mediterranean myoclonus. These were considered to be different syndromes, based on differences in onset and severity, however they were later confirmed to be the same disease (Malafosse et al. 1992). Recognizing the research of Unverricht and Lundborg, the syndrome is known as Unverricht-Lundborg disease, however the name EPM1 (OMIM254800) is also used. EPM1 is considered part of the Finnish disease heritage, a group of rare genetic disorders enriched in the Finnish population due to founder effects and genetic isolation (Norio 2003). The disease is recessively inherited, and its incidence in Finland is 1 in 20 000 births (Norio, Koskiniemi 1979). It is also part of the group of PME disorders, characterised by their common features of progressive neurological decline, myoclonus and epilepsy, with EPM1 the single most common cause for PME. Other diseases classified as PMEs include type I sialidosis, myoclonus epilepsy and ragged red fibres (MERRF syndrome), Lafora disease and neuronal ceroid lipofuscinoses (Berkovic, So & Andermann 1991). EPM1 is considered underdiagnosed around the world due to its rare nature, need for genetic diagnosis and symptoms that are reminiscent of other PMEs and juvenile myoclonic epilepsy (Kälviäinen et al. 2008, de Haan et al. 2004).

Table 1. The etiological classification of epilepsies adapted from Shorvon (2011) (Shorvon 2011)

Main category:	**Subcategories:**
Idiopathic epilepsy	Pure epilepsies due to single gene disorders
	Pure epilepsies with complex inheritance
Symptomatic epilepsy: Predominately genetic or developmental causation	Childhood epilepsy syndromes
	Progressive myoclonic epilepsies **(EPM1)**
	Neurocutaneous syndromes
	Other neurologic single gene disorders
	Disorders of chromosome function
	Developmental anomalies of cerebral structure
Symptomatic epilepsy: Predominately acquired causation	Hippocampal sclerosis
	Perinatal and infantile causes
	Cerebral trauma
	Cerebral tumour
	Cerebral infection
	Cerebrovascular disorders
	Cerebral immunologic disorders
	Degenerative and other neurologic conditions
Provoked epilepsy	Varied provoking factors
	Reflex epilepsies
Cryptogenic epilepsies	

1.2.1 Clinical presentation and course of the disease

The onset of EPM1 is typically between 6 to 16 years of age and the manifesting symptoms are most often tonic-clonic epileptic seizures or stimulus sensitive involuntary myoclonic jerks, provoked by action, lights or sound (Koskiniemi et al. 1974, Norio, Koskiniemi 1979). As the disease advances, other symptoms including ataxia, incoordination, intentional tremor, and dysarthria emerge (Kälviäinen et al.

2008). The myoclonus becomes more severe and the clinical state of the patients declines for 5-10 years, before the disease progression stabilizes (Magaudda et al. 2006). The epileptic seizures can be controlled with anti-epileptic drugs, namely valproic acid, clonazepam, piracetam, levetiracetam, topiramate and zonisamide (Kälviäinen et al. 2008, Roivainen, Karvonen & Puumala 2014), however the myoclonus and ataxia present in the disease remains resistant to the treatment[47]. Thus, the mainstay of EPM1 treatment is continuing psychological and rehabilitive support to the patients throughout their life, combined with anticonvulsant medication (Kälviäinen et al. 2008). The severity of the symptoms varies, with some patients rendered wheelchair bound by the severe ataxia and myoclonus while other remain virtually asymptomatic. With appropriate treatment, the life expectancy of the patients is approximately normal (Kälviäinen et al. 2008).

1.2.2 Neuropathological findings in EPM1 patients

Neuropathological data on EPM1 are scarce, and the available findings are heterogeneous. Part of this can be attributed to the deleterious effect of the previous phenytoin therapy, which is known to cause extensive cerebellar atrophy in the patients (Eldridge et al. 1983). The patients show loss of cerebellar granular cells and Purkinje cells (Eldridge et al. 1983)as well as neuron loss in the cortices, striatum, thalamus and brainstem (Mascalchi et al. 2002, Koskenkorva et al. 2009, Cohen et al. 2011, Koskiniemi et al. 1974)with changes also reported in spinal motor neurons (Eldridge et al. 1983). Imaging studies in EPM1 have demonstrated a range of changes in the brain. At the onset of the disease, patient MRI does not show any abnormalities, and changes become evident once the disease progresses (Kälviäinen et al. 2008). Most studies report cerebral atrophy and cerebral cortices are shown to undergo atrophy on sensory, motor and somatosensory regions (Koskenkorva et al. 2012, Koskenkorva et al. 2009, Mascalchi et al. 2002). The severity of the myoclonus in patients has been shown to correlate with the cortical thinning present in the disease (Koskenkorva et al. 2012), and the changes in dopaminergic function are thought to contribute to the severely incapacitating myoclonus present in the disease (Korja et al. 2007b, Danner et al. 2013, Mervaala et al. 1986). Combined with the reported striatal and thalamic (Korja et al. 2007b) changes, the myoclonus and motor disturbances present in the patients have been considered to be of cortical origin (Koskenkorva et al. 2009) and augmented by the damaged thalamocortical circuitry (Suoranta et al. 2013).

1.2.3 Bone findings in EPM1 patients

Besides the neurological pathologies, diffuse thickening of the skull and scoliosis (Koskiniemi et al. 1974) and more specifically *hyperostosis frontalis interna* (Korja et al. 2007a) have been reported in EPM1 patients. In line with the findings skull thickening, a transcranial magnetic stimulation study reported the distance from scalp to cortex to be longer in EPM1 patients (Danner et al. 2013). A study involving 66 EPM1 patients showed that all patients exhibit diffuse thickening of cranial bones, with 61% also showing other skeletal changes, most commonly arachnodactaly, scoliosis, enlarged sinuses, and accessory ossicles of the foot (Suoranta et al. 2012). The underlying cause for diverse bone changes found in EPM1 patients is currently unknown.

1.2.4 Cystatin B (CSTB)

Recessive mutations of the cystatin B (*CSTB*) gene underlie EPM1 (Pennacchio et al. 1996), however, how these defects precicely lead to the observed symptoms is currently unclear. Presently, 14 causative expansion mutations have been identified (Pennacchio et al. 1996, Pinto et al. 2012, Lalioti et al. 1997, Joensuu, Lehesjoki & Kopra 2008). No genotype-phenotype correlation is known to exist, however compound heterozygote patients suffer from a more severe disease phenotype (Koskenkorva et al. 2011). The *CSTB* gene encodes protein cystatin B (CSTB, sometimes also referred to as stefin B) (Pennacchio et al. 1996, Ritonja, Machleidt & Barrett 1985), an inhibitor of lysosomal cysteine cathepsins, including cathepsin H, L, S, B and K (Green et al. 1984, Bromme, Rinne & Kirschke 1991). As Cat K has an vital role in bone resorption by osteoclasts (Kiviranta et al. 2005), inadequate inhibition of cat K could possibly play a part in the bone changes observed in patients. CSTB is known to be ubiquitously expressed in a variety of cell types and tissues, and has been shown to be expressed both in neurons and glial cells (Kominami et al. 1984, Okuneva et al. 2015). Kindling induced status epilepticus has also been shown to upregulate *Cstb* expression in rats (D'Amato et al. 2000).

1.2.5 Mouse model of EPM1

Due to the highly preserved nature of basic neuronal structure, much of neuroscientific research is conducted with model organisms. The nematode *Caenorhabditis elegans* is frequently used in the modelling and study of the nervous system due to its simple and thoroughly documented neuronal architecture and well known neuron development and connectivity (Sasakura et al. 2013). Fruit flies (*Drosophilae melanogaster*) are used due to the easy production of genetically modified models and their clearly identifiable phenotypes and are thus used as a model organism in

basic research of gene and protein function (Bellen, Tong & Tsuda 2010). Zebra fish (*Danio rerio*) are often used as a behavioral model due to their easily observable and quantifiable developmental behaviors and as a developmental model, as their embryonic development is rapid and easily observable (Clay, Coughlin 2015). At the other end of the spectrum of model organisms are non-human primates, such as rhesus macaques, which are utilised due to their extremely similar genetic background and brain structure as humans, up to the point that even enables studies on evolution of language (Fisher, Marcus 2006).

In this thesis work, as very often in neuroscience, the model organism of choice is the mouse (*Mus musculus*). The genome of mice can be genetically modified to provide models of human disease through altering the expression of existing genes by silencing or over-expressing them or by introducing new genes into the genome. Mice also reproduce rapidly and their anatomy, genome and cell biology has been extensively studied (Harper 2010). Mice share 97% of their genome with that of humans and as a mammalian model, the mouse brain structure is very compatible for research in neuroscience (Harper 2010). Therefore they are extensively used in the study of diseases such as Alzheimer's (Lau et al. 2008), Parkinson's (Morin, Jourdain & Di Paolo 2014), and epilepsy (Harward, McNamara 2014), among many other neurological disorders (Nguyen, Xu 2008, Harper 2010). Nevertheless, due to the difference between the species in genetics, neuroanatomy and neurobiology, they never as such reproduce the complete phenotype of any human disorder (Morrissette et al. 2009, Harper 2010)and are, *per se,* only a model for studying disease processes.

After the underlying gene for EPM1 was identified, a knock-out mouse model (the *Cstb*$^{-/-}$ mice) for the disease was generated (Pennacchio et al. 1998). The model was generated by disrupting the reading frame of the mouse *Cstb* gene with an insertion of a neomysin cassette into the first exon, leading to an almost complete loss of the *Cstb* protein (Pennacchio et al. 1998). The mouse model has been shown to recapitulate the patient phenotype well, with myoclonus manifesting at the age of one month and ataxia emerging at the age of six months (Pennacchio et al. 1998). Unlike the stimulus sensitive myoclonus in patients (Kälviäinen et al. 2008), myoclonus in mice only manifests during sleep (Pennacchio et al. 1998), and can be so robust that it causes the animals to jump into the air (personal observation).

The model replicates the cerebellar and cerebral atrophy as well as the loss of cerebellar granule cells and neurons observed in patients (Shannon et al. 2002, Pennacchio et al. 1998, Tegelberg et al. 2012). Atrophy and selective neuron loss have been shown to affect the thalamocortical system, hippocampus and entorhinal cortex, with loss of cortical neurons preceding the changes in the corresponding thalamic nuclei (Shannon et al. 2002, Tegelberg et al. 2012). The atrophy and volume loss in the cortex and cerebellum are progressive (Tegelberg et al. 2012) and the brain of the

mice is smaller compared to controls (**Figure 4**). The brain weighs approximately 25% less compared to controls, although no difference in the brain/body weight ratio is observed (Shannon et al. 2002). Histology in the *Cstb*$^{-/-}$ mouse has shown extensive gliosis, especially in the WM (Shannon et al. 2002)and gene expression analysis indicates upregulation of glial activation genes in 8-month-old animals (Lieuallen et al. 2001). At 1 month, increased expression of immune and defence response genes is also observed (Joensuu et al. 2014). These findings are in line with the early and spreading microglial activation, seen already at p14, which precedes the astroglial activation, neuron loss and myoclonus that manifest in the early stages of the disease (Tegelberg et al. 2012). The cultured microglia demonstrate higher expression of *Cstb* mRNA compared to astroglia and neurons, and CSTB deficiency has been linked to altered function of microglia in the *Cstb*$^{-/-}$ mice (Okuneva et al. 2015).

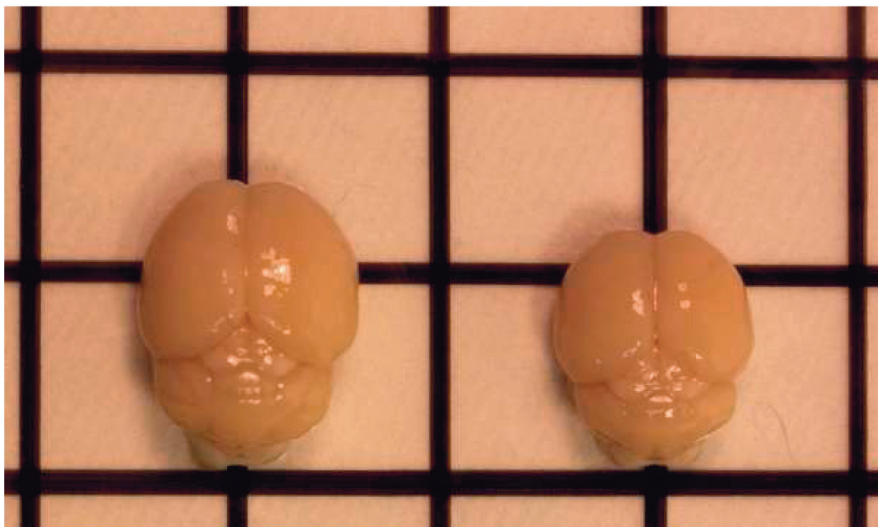

Figure 4. Cstb$^{-/-}$ mice are used as an EPM1 model in the study of the disease. EPM1 mouse model recapitulates well the clinical symptoms seen in patients, with the onset of ataxia at 1 month and myoclonus at 6 months of age. The atrophy seen in the patients manifests also in the animal model and the picture illustrates the degree of volume loss in *Cstb*$^{-/-}$ brain at 6 months, with a brain from a healthy control on the left, and a *Cstb*$^{-/-}$ brain on the right. One square represents 1 cm^2. Picture by Saara Tegelberg.

The hippocampus of a *Cstb*$^{-/-}$ mouse shows latent hyperexcitability, likely due to loss of GABAergic inhibition (Buzzi et al. 2012, Franceschetti et al. 2007). Changes in GABAergic signalling pathways can already be observed at early stages of the disease, and in immunohistochemistry, *Cstb*$^{-/-}$ mouse neurons show less GABAergic terminals compared to controls (Joensuu et al. 2014). This is likely to contribute to

the observed hyperexcitable phenotype, as histopathology from an EPM1 patient shows similar results (Buzzi et al. 2012). Histology and cell cultures have indicated that oxidative stress plays a role in the pathogenesis (Lehtinen et al. 2009). Altered tryptophan metabolism has also been reported in *Cstb*$^{-/-}$ mice (Vaarmann, Kaasik & Zharkovsky 2006), however the principal disease cascade leading to the observed pathological changes remains to be elucidated.

1.3 BASICS IN BIOLOGICAL IMAGING

"If the hand be held between the discharge-tube and the screen, the darker shadow of the bones is seen within the slightly dark shadow-image of the hand itself... For brevity's sake I shall use the expression 'rays'; and to distinguish them from others of this name I shall call them 'X-rays'."

- Wilhelm Röntgen-

In biological research, visualization of the different structural or functional properties of organisms is essential. Biological imaging is an umbrella term that refers to methods used in visualising different aspects of biological systems. The oldest, and still most widely used biological imaging method is light microscopy, based on the use of visible light and magnifying lenses. It enables the study of structures too small to view with a naked eye, facilitating for instance the discovery of cells by Robert Hooke in 1665 (Hooke 1665). The value of biological imaging methods in research has been readily appreciated, with the first Nobel price in physics given to Wilhelm Röntgen for the discovery of x-rays and their use in imaging (Nobel Lectures Physics 1901–1921). Biological imaging methods often start as tools for research, but find their way into medical applications, as rapidly happened with Röntgen's invention, and subsequently, with many other imaging modalities.

Currently, a range of biological imaging methods is used in neuroscience in both clinical work and research. Cranial ultrasound is often used to study the brain of neonates as the the open sutures of the skull allow good penetrance for the sound waves, and this approach has been for instance used in investigating brain damage in preterm babies (Plaisier et al. 2015). Through the use of radioisotopes, positron emission tomography provides information concerning brain function through metabolic indications such as mapping hypoactivity of different brain regions in epileptic patients through their respective local glucose consumption (Akman et al. 2015).

Magnetic resonance imaging (MRI) is a widely used imaging method that is based on nuclear magnetic resonance (NMR) as it can provide anatomical information, such as the imaging of tumors (Castillo 2014), or functional information on brain activity in functional MRI, or (fMRI) through changes in local haemodynamics for instance in investigating language centres in the brain (Gelinas et al. 2014). Magnetic resonance spectroscopy (MRS) can provide metabolic information using a MRI system, such as determining GABA concentrations in the thalamus of juvenile myoclonic epilepsy patients (Hattingen et al. 2014). Beside the use of x-ray imaging in investigating bone, like MRI, x-ray computed tomography (CT) is widely used in anatomical neuroimaging due to its versatility, and due to high anatomical resolution and the speed of acquisition it is for instance utilized in imaging of acute trauma cases (Semelka et al. 2007) and investigation of vasculature (Ravindra et al. 2015). Functional information can be obtained in optical imaging, such as observing the neurovasculature and blood oxidation for mapping seizure foci in neonates (Singh et al. 2014). Magnetoencephalography (MEG) is based on detecting magnetic fields produced by electric signals in the brain and can for instance be utilized in mapping cortical inhibitory activity (Danner et al. 2013). In this thesis, in addition to light microscopy, other imaging modalities, such as MRI, CT, and electron microscopy, were utilized. Their basic principles and applications will be described in more detail in the following chapters.

1.3.1 Principles of magnetic resonance imaging

Magnetic resonance imaging, or MRI, is a widely used medical imaging method that is based on NMR. It can provide anatomical, functional or metabolic information about the target tissue. Due to the extensive electromagnetic and quantum mechanical theoretical background behind the method, the basis of MRI and NMR is not usually explained to the full extent of the theory and is rather described with a simplified portrayal. The description given here has been adapted from the portrayal originally given by Gadian (Gadian 1995).

MRI is most commonly centred on observing hydrogen protons (^{1}H) based on two physical properties of the atoms, their electrical charge, and their quantum mechanical property of spin, which can be described as angular rotary momentum of the particle against its axis. According to the law of physics, electrical charge in motion creates a magnetic field, and thus the nuclear spins could be visualized as small spinning bar magnets. As a quantum mechanical property, the spin values are not continuous and rather they can only have defined values. Therefore, when placed in an external magnetic field, a molecule with a spin number ½ can align itself in one of two states. One is the low energy state of the spin, with the positive pole

aligned against the negative in the field, and the other, a high-energy state in which the positive nuclear pole faces the field.

Thus the nuclear magnet (the spin), when placed in an external magnetic field, can switch from its low energy state to its high-energy state by absorbing energy from a photon. Correspondingly, switching from high to low energy state emits a photon of equal energy. This switching of spin states is called transition, and it can be induced with an electromagnetic pulse of radiowave frequency. Thus, when the spins in a magnetic field are subject to a radio frequency pulse of correct frequency, the energy states of these spins change. This results, depending on the original state of the spins, in both absorption and emission of photons. The resonance frequency is called the Larmour-frequency and it is unique for each nuclei and strength of the external magnetic field.

If the number of spins in the high and low energy states would be equal, the number of emitted and absorbed photons after a transition would also be equal and no change in overall magnetisation would be observed. Due to the small energy difference between the low and high states the difference in spin populations is miniscule, one in ten thousand spins. The difference is still enough to yield a change in overall energy during transition, and can be observed with a radio frequency coil when the system returns towards equilibrium. The population difference is directly proportional to the magnetic field strength, and the amount of signal depends on the numbers of protons on the excited area. Thus the observed area must be large enough and contain enough protons to create a measurable signal.

In order to observe complex three-dimensional structures with MRI, the signal originating from different points in space along three axes has to be differentiated. In a magnetic field with a field gradient, protons in different regions along the gradient are subject to different field strengths. Since the resonance frequency of the protons depends on the strength of the magnetic field, the resonance frequency of the protons also depends on the position of the protons along the field gradient. Thus, a radio frequency pulse on specific frequency excites only a specific portioning of protons along the gradient. The signal is thus received from a specific area along the gradient and provides spatial resolution along one axis, which here shall be addressed as axis Z.

After the imaging slice direction on the Z-axis has been exited using a radio frequency pulse, the nuclei in that specific plane resonate on a frequency specific to the field strength (Larmour frequency) in common phase. If the protons in the plane are then subjected to a field gradient in a direction of the X-axis, the spins start to rotate with a resonance frequency corresponding to their position on the X-axis. When the field gradient on the X-axis is turned off and magnetisation returns, all the resonating spins rotate at same frequency, but in a different phase, which corresponds with their localisation along the X-axis. Therefore, localisation of the spins along the

X-axis can be determined by observing the phase of the spins. This is called phase encoding. Finally the plane is subjected to a field gradient along the Y-axis, so that a difference in the frequency of the spins along this axis is acquired, and technique for determining the source of the signal along the in three-dimensional space is achieved.

A two-dimensional image is composed of pixels, but MRI is usually utilized for studying three-dimensional structures, in which images consist of pixels, that also contain volume information, or "voxels". These represent a certain volume of the tissue or structure that is studied and represent the amount of signal acquired with a radio frequency coil from this volume. The signal is most commonly acquired from protons that are present in tissue water, fats or other hydrogen rich compounds. After excitation with radiofrequency pulse, the protons revert back to their original state in a process called relaxation. Each tissue type is characterized by their individual relaxation times for both longitudinal relaxation (T1), and transverse relaxation (T2) and the use of imaging sequences sensitive to these relaxation times provide a way to discern wide range of tissues. Images in which main source of the contrast is from T1 relaxation are called T1-weighted, and ones with predominantly T2 based signal are referred to as T2-weighted. Use of sequence that minimize the effect of differences in T1 and T2 times produces an image in which the contrast is based on the proton density of the tissue. These are called proton density weighted images. The acquisition process of signal from tissue involves intricate manipulation of magnetic fields and radio frequency pulses and reconstructing the images requires elaborate signal processing, but these are based on the principles described here.

MRI has wide range of applications, and is routinely used in clinical and research settings, in which MRI systems are commonly utilized for obtaining anatomical information. Examples of these uses include pre-surgical investigation of lesions in epilepsy surgery patients (Holthausen, Pieper & Kudernatsch 2013) or tumours (Castillo 2014). Using an MRI system, MRS can also be performed for acquiring metabolic information about tissues, such as obtaining information about cortical N-acetyl-aspartate levels in NCL patients (Worgall et al. 2007). Information about brain activity can be obtained in fMRI by following changes in local blood flow and oxidation and this method can be used for instance in pre-operatic mapping of hemispheric language dominance in epilepsy surgery patients (Gelinas et al. 2014). Use of interventional MRI is also emerging with operations like MRI navigated transurethral prostate cancer treatments (Ghai, Trachtenberg 2015). A widely used MRI method called diffusion weighted imaging provides information the about movement of water in tissue and its principles and uses are described in more detail in the following chapter.

1.3.2 Diffusion weighted imaging

Acquiring information on the diffusion of molecules, usually water, in tissue using an MRI system is called diffusion weighted imaging (DWI). The explanation of DWI and its principles given here have been adapted from the portrayal originally given by Mori (Mori 2007). Water molecules in tissue are in constant movement due to Brownian motion, and an MRI system can be used to acquire signal from protons in water. In brief, diffusion information is acquired by using a pulse to dephase the spins in the area of image acquisition, after which a time for diffusion of water is allowed. Before acquiring the signal, a rephasing pulse is used to rephase the spins in the area of acquisition. In a scenario where no diffusion of water has happened, all the spins are rephased and the same total amount of signal is acquired. Diffusion causes some of the water that could have been re-phased move out of the plane, leading to signal attenuation. Loss of signal is proportional to the amount of diffusion happening in the plane. This provides information about the diffusion in one direction along the phase-encoded axis, meaning that the measurement must be repeated for all three gradient directions to obtain three-dimensional diffusion information, which can be used for instance in calculating average diffusivity per voxel.

DWI is commonly utilised for obtaining information about tissue microstructure that affects the diffusion characteristics of water. From data acquired using DWI, representations of diffusion in tissue can be calculated. This information is often presented in the form of tensor, leading to the common use of term diffusion tensor imaging (DTI). For calculating diffusion tensors, diffusion information from at least 6 directions is required. In the tensor model, the diffusion of water in three-dimensional space is represented with three orthogonal tensors: lambda 1, lambda 2, and lambda 3. Common DTI parameters calculated from these tensors include the diffusion along the main axis of diffusion, referred to as axial diffusion (AD), diffusion on the plane parallel to the main axis, referred to as radial diffusion (RD) and a calculated mean of these two, mean diffusivity (MD). Anisotropy of diffusion indicates how variable the diffusion is in different directions and is commonly represented by the parameter fractional anisotropy (FA). It is a scalar value, calculated out of DTI data, and can range from 0 for isotropic, unrestricted/equally restricted to 1, for to anisotropic, or totally restricted to all but one direction (**Figure 5**). Pathological processes in the brain often cause rapid changes in local diffusion dynamics, which makes DTI a sensitive and acute way of obtaining information about the affected tissue. Since water diffuses more freely parallel to axons than perpendicular to them, FA is a robust indicator of pathological processes. It can easily be compared between subjects and is commonly used as a marker of WM integrity (Liu et al. 2011, Burzynska et al. 2010, Damoiseaux et al. 2009) as decreased FA combined with increase of RD (and possible decreased AD) is observed with loss of fibre or demyelination (Concha et

al. 2006, Sun et al. 2008). This is thought to result from increase in axonal spacing (Sen, Basser 2005). To name few examples, DTI has been used in study of white matter abnormalities in focal epilepsy patients (Campos et al. 2015), investigating WM integrity in ischemic stroke patients (Dacosta-Aguayo et al. 2014) and WM changes in Alzheimer's (Li et al. 2015), among many other uses. DTI is also used in animal models of neurodegenerative disease, and has been used for instance to investigate the progression of WM changes in traumatic brain injury in rats (Begonia et al. 2014), following neonatal hippocampal lesions in macaques (Meng et al. 2014) and assessing myelin damage in a mouse model of spinal cord injury (Tu et al. 2013).

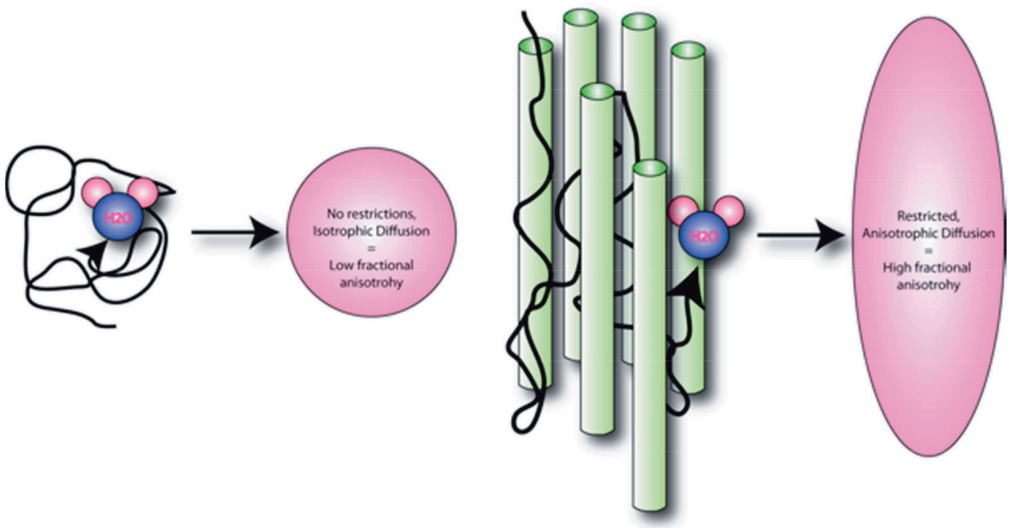

Figure 5. Fractional anisotropy reflects restrictions of diffusion due to tissue microstructure. Fractional anisotropy reflects the effect of tissue microstructure on the diffusion of water in tissue. When the diffusion of water is not restricted in any direction, this accounts for isotropic diffusion, whereas tissue microstructure, such as axon bundles in white matter restrict diffusion of water in certain directions, which causes highly restricted diffusion that is reflected by high fractional anisotropy.

1.3.3 Track-based spatial statistics

Analysing complex three-dimensional datasets, such as whole brain FA data, is very labour-intensive when done manually. This often leads to the restriction of analysed areas and the use of a region of interest (ROI) based approach. In such cases the research hypothesis dictates which areas are analysed. Restricting the areas of analysis based on the hypothesis however overlooks changes in areas previously unknown or not assumed to be affected. Reproducible and bias-free ROI selection in different sized or atrophied subjects also requires a high degree of anatomical

expertise. This has prompted the need for automated analysis of 3D imaging data. One such method in brain imaging is tract-based spatial statistics (TBSS) analysis (Smith et al. 2006, Smith et al. 2007). In this method, all whole brain FA-maps that are compared are brought into a common 3D-space for voxel by voxel group level statistical comparison of FA-values. In the method the FA-maps of brains are cross-compared to find the most representative brain of the groups, in order to minimize the need for warping individual brains when brought into a common 3D space. The most representative brain is then selected to be used as a template, into which the rest of the FA-maps are co-registered to using affine and non-linear transformations. This representation of the whole brain is then averaged into a mean FA image of the whole group. As the WM tracts have high FA-values, by setting a threshold the FA-values the mean brain can be used to form an FA-skeleton representing the major WM-tracts. All analysed brains are skeletonized with the same threshold. After this, all individual FA-skeletons are aligned to the template using affine transformations and centers of the WM-tracts are co-aligned on the template skeleton. As all the FA-maps have been brought to a common 3D-space and the WM-tracts aligned, FA-values of each voxel can be statistically compared. The method can be also used for analysing other measures of diffusion, AD, RD or MD, to complement the FA analysis. AD indicates diffusion in the primary direction of diffusion, RD the diffusion along the two minor directions and MD indicates mean diffusion of all directions combined.

As TBSS is a group level analysis method, it has only limited clinical diagnostic use. However, in research settings it has been demonstrated to be effective in identifying WM changes in numerous neurodegenerative disorders. For example, in a study of mild cognitive decline and Alzheimer's, TBSS analysis revealed decreased anatomical connectivity (Damoiseaux et al. 2009), and a study in Parkinson's connected the olfactory dysfunction present in the disease to WM changes (Ibarretxe-Bilbao et al. 2010). In juvenile myoclonic epilepsy, TBSS revealed widespread WM abnormality (Focke et al. 2014) and demonstrated parallel changes in temporal lobe epilepsy (Focke et al. 2008). TBSS has also been used in a longitudinal settings, and an investigation of Huntington's disease was able to demonstrate progressive decline in WM integrity over a course of 30 months (Poudel et al. 2015).

The method was developed for analysing patient data, but with modifications the analysis can also be utilized in animal models. A study in a kainite model of epilepsy in rats revealed novel affected areas and confirmed tissue level changes associated with observed changes in diffusion (Sierra et al. 2011) and TBSS analysis of correlating changes in FA to the lack of myelin in a model of Pelizaeus-Merzbacher disease demonstrated the use of the method in mice (Ruest et al. 2011). TBSS has also been performed in non-human primates, and study in macaques was able to connect hippocampal WM-lesions to deficits in memory function (Meng et al. 2014).

1.3.4 X-ray computed tomography

Imaging techniques that provide sectional (tomographic) information through the use of penetrating waves (i.e. X-rays, gamma rays) are called tomographies, and the most commonly used method is x-ray computed tomography (CT). The method is extensively used in medical imaging, in addition to which it is widely utilized for example in security scanners, industrial radiography, archaeology and material physics. The explanation of its principles given here has been adapted from a book by Soimakallio et al. (Soimakallio et al. 2005).

Different tissues, such as muscle, bone or fat have distinctive radiodensities, described by their Hounsfield unit values. When a x-ray beam is passed through a body or limb and detected at the other side, differences in the amount of absorbed x-rays by various tissues provide contrast and allows distinguishing between different structures. In CT, a series of two-dimensional x-ray images are acquired from different directions on a single axis of rotation, usually covering a 180-degree arc of the object of interest (**Figure 6**). Images from different angles are obtained either by moving the sensor around the target or by rotating the target. The back-projection principle is then utilised in calculating a three-dimensional presentation from the series of two-dimensional images.

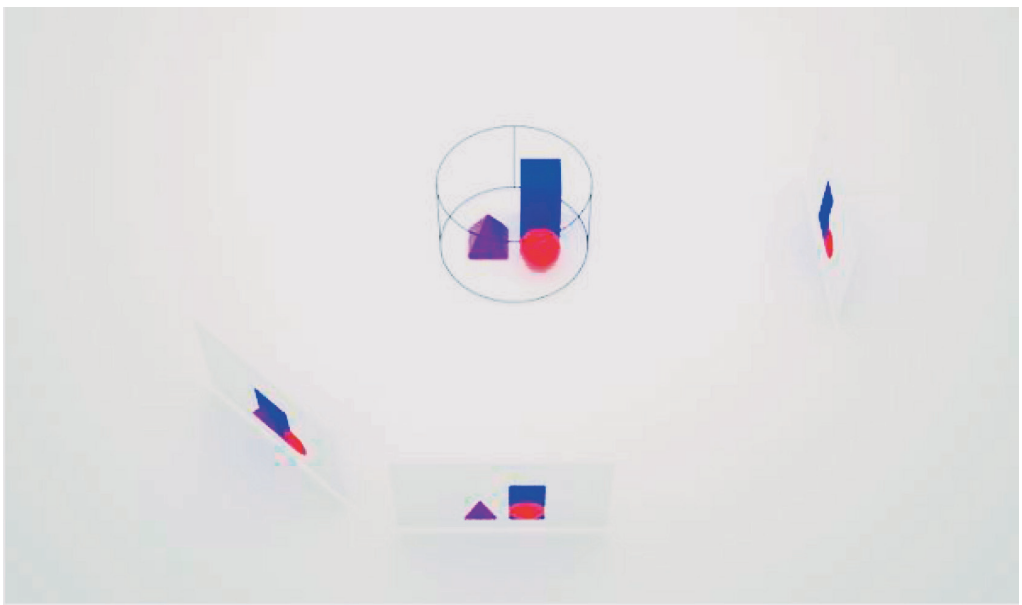

Figure 6. Simplified principle of computed tomography. A series of two-dimensional x-ray images are acquired from different directions on a single axis of rotation, either by moving the sensor around the target or by rotating the target. The back-projection principle is subsequently utilised in calculating a three-dimensional presentation from the series of two-dimensional images. Picture by Joonas Saaranen

While the need for ionizing radiation limits the usage of CT, it is still widely used in clinical settings and research. Whole body CT scans are performed for instance for trauma patients (Caputo et al. 2014) and brain CT is a common way of studying head trauma (Haydel et al. 2000). CT is also utilized in the study of bone structure, such as investigations of bone mineral density (BMD) (Schreiber, Anderson & Hsu 2014). X-ray tomography that reaches micrometre scale resolution is referred as microtomography (μCT) (**Figure 7**). Microtomography is also used in preclinical animal research, and has for instance been used as in the study of bone microstructure in a mouse model of thalassemia (Vogiatzi et al. 2010) and in the investigation of changes in bone mass and composition in a mouse model of obesity (Zhang et al. 2015).

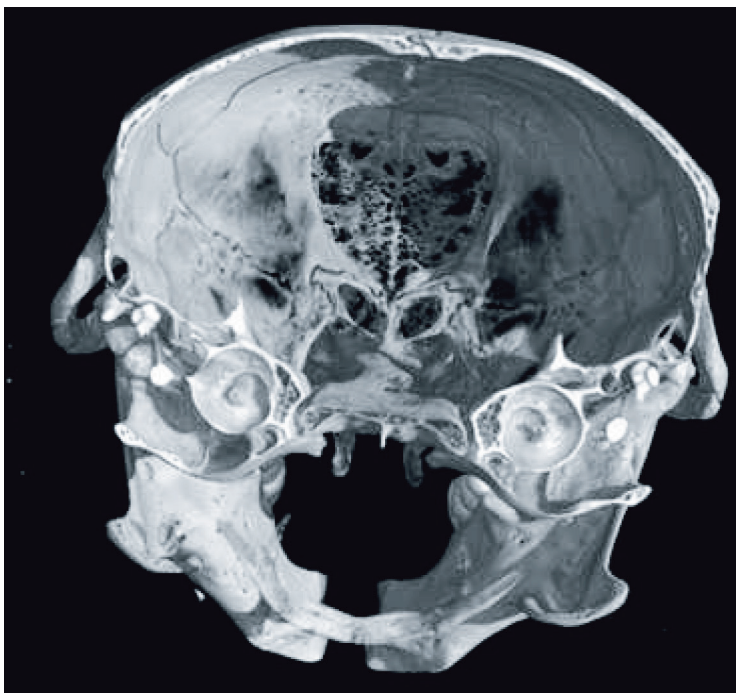

Figure 7. Computed tomography image of a mouse skull. A cross-sectional cut of a μCT-image of a mouse skull shows the conch-shaped inner ear in the middle of the image, and the detail in the fine structure of the trabecular bone demonstrates the resolution obtained with microtomography system. The voxel size in this reconstruction is 10x10x10 μm.

1.3.5 Transmission electron microscopy

The magnification achieved with conventional light microscopy is limited by the wavelength of photons in visible light and the resolution is not sufficient for viewing many subcellular structures. In these cases electron microscopes are used. Electron microscopes use accelerated electron beams for detection instead of visible light, and as electrons have much lower wavelength than visible light, electron transmission based detection can be utilized in visualizing much smaller structures, up to a resolution enabling the viewing of atoms (Pennycook 2012). The following simplified explanation of transmission electron microscopy (TEM) has been adapted from Williams and Carter (Williams, Carter 2009).

In transmission electron microscopy, a condensed electron beam, usually generated with a tungsten filament, is directed at a sample under vacuum. Samples are ultra thin sections of material or tissue, prepared using a microtome. In light microscopy, the visibility of certain structures is enhanced using stains that absorb light, and create contrast to the image. For TEM, compounds of heavy metals such as osmium, lead or uranium are used for staining. In bright field TEM, as the beam passes through the sample, the stain absorbs or diffracts electrons and thus highlights certain cellular regions or structures of interest. After passing through the sample, the electron beam is magnified and focused to form a coherent image, then captured with an imaging device, such as camera. Different systems of contrast formation are used, depending on the desired magnification and the studied sample. Due to the high magnifications obtained with TEM, the method is used for instance in nanotechnology for analysing particle size and geometry (Korbekandi et al. 2015), in virology for the investigation of infective properties of a hepatitis virus (Liu et al. 2014) and in histopathology for the investigation of cellular scale structures (Kuronen et al. 2012).

2 AIMS OF THE STUDY

The overall aim of this study was to elucidate the events contributing to the progression of progressive myoclonus epilepsy, EPM1, in an experimental mouse model, the *Cstb*$^{-/-}$ mouse.

The specific aims of the study were:

Aim 1. To gain a comprehensive picture of EPM1 disease progression by conducting longitudinal MRI and DTI follow-up studies in *Cstb*$^{-/-}$ mice from pre-symptomatic to fully symptomatic stage (1-6 months).

Aim 2. To investigate white matter (WM) changes in adult (6-month-old) *Cstb*$^{-/-}$ mice and evaluate the congruence of the findings in adult EPM1 patients.

Aim 3. To evaluate the contribution of defective cystatin B function on bone pathology, metabolism and properties of osteoclasts in the *Cstb*$^{-/-}$ mouse using microtomography, bone histology and bone marrow derived osteoclast cultures.

3 MATERIALS AND METHODS

3.1 *CSTB*$^{-/-}$ MOUSE (I,II,III)

Cystatin B-deficient mice (*Cstb*$^{-/-}$) (Pennacchio et al. 1998) were used as an animal model of EPM1 in this study. The mice were obtained from the Jackson Laboratory (129-*Cstb*^{tm1Rm}/J; stock #003486) and age- and gender matched 129SvJ wild-type mice served as controls. Animal experiments were approved by State Provincial Office of Southern Finland (ESLH-2007-05788/Ym-23: ESAVI-2010-07744/ Ym-23/ ESAVI-7039/04.10.03/2013).

3.2 MAGNETIC RESONANCE IMAGING (I,II)

3.2.1 MRI volumetry (I)

In vivo MRI volumetry was performed on four *Cstb*$^{-/-}$ and four control female mice. Volumetry data were acquired at the age of 1, 2, 4 and 6 months. Animals were imaged under isoflurane anaesthetisia (1% isoflurane in 70% N_2O / 30% O_2,) and the body temperature was maintained at 37°C throughout imaging. A 4.7 T Varian UNITY INOVA MRI system and an actively-decoupled volume coil-quadrature surface coil set (Rapid Biomedical GmbH, Rimpar, Germany) was used for image acquisition. An adiabatic multi-slice spin echo sequence was used for acquiring anatomical images for volumetric analysis (**Figure 8**) (17 slices, 100 x 100 μm in-plane resolution; matrix 256x256, slice thickness 0.75 mm, TE 20, 40 and 60 ms, TR 1.8 s, echo train length (NT) 4). A mean image was averaged out of 3 TEs. ROIs were drawn on blinded data sets according to the mouse brain atlas (Franklin, Paxinos 1997) using in-house-buildt software Aedes 1.0. (Niskanen)(**Figure 8**). ROIs were drawn for the whole brain (excluding medulla), cerebellum, cerebral cortices, striatum and hippocampus for each time point. Statistical comparison was done using one-way analysis of variance (ANOVA) with Bonferroni post hoc correction.

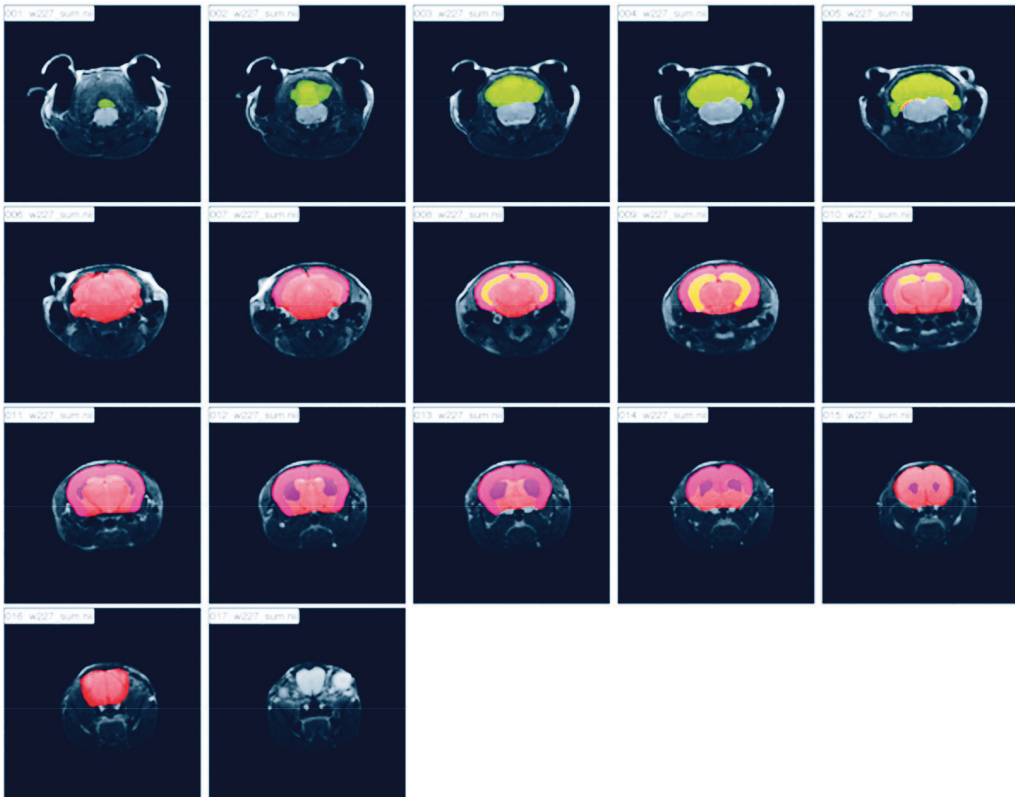

Figure 8. ROI selection in in vivo volumetry. The image shows the ROIs for whole brain volume (red), striatum (purple), cortices (pink), hippocampus (yellow) and cerebellum (green) overlaid on the MR image stack of a 6-month-old control mouse brain.

3.2.3 Ex vivo diffusion tensor imaging (I,II)

3.2.3.1 Sample preparation (I,II)

For *ex vivo* brain DTI, we used 2-months-old (9 *Cstb*$^{-/-}$; 6 female, 7 controls; 4 female), 4-months-old (9 *Cstb*$^{-/-}$; 5 female, 6 controls; 2 female) and 6-months-old (9 *Cstb*$^{-/-}$; 8 female, 4 controls; all female) mice. Animals were anaesthetized with pentobarbital (Mebunat, 80-150 mg/kg *ip*, Orion, Finland) and intracardially perfused with PBS and sodium heparin (0.16ug/ml, Sigma), and then perfusion fixed with 4% paraformaldehyde (PFA) (4% by volume, Sigma) in phosphate buffered saline (PBS). The brains were then removed, and postfixed for 24h. The brains were then immersed in perfluoropolyether (Fomblin® LC08, Solway Solexis,) for *ex vivo* DTI.

3.2.3.2 Ex vivo DTI (I,II)

Imaging of the brains was performed with a 9.4 T vertical magnet (Oxford Instruments, Abingdon, UK) using a Varian DirectDrive console (Varian Inc. Palo Alto, USA). Data were acquired using a 3D fast spin echo sequence (echo time (TE) 28 ms, repetition time (TR) 1000 ms, matrix 128×64×64, zero padded to 256×128×128, field of view (FOV) 20×10×10 mm^3, echo train length = 2) and six individual 3D data sets with diffusion weighting in six orthogonal directions (diffusion time 17 ms, *b*-value 1000 s/ mm^2). One reference data set without diffusion weighting was also obtained. Acquisition of one dataset took 16 hours.

3.2.3.3 Track based spatial statistics (I,II)

The TBSS analysis was performed as described in the original publications (Smith et al. 2006, Smith et al. 2007) with the modifications for use in rodents (Sierra et al. 2011). First, the acquired DTI data were corrected for eddy current distortions using affine (linear) alignment with FMRIB's Linear Image Registration Tool (FLIRT) (Jenkinson et al. 2002, Jenkinson, Smith 2001). The diffusion tensor model was calculated using a DTIFIT (Smith et al. 2004) program and resulting individual FA maps underwent the TBSS analysis.

When we studied the development of WM-changes (I), the analysis of the data was performed with hemisphere-mirroring. The aim of hemisphere mirroring, as previously stated (Sierra et al. 2011) was to gain a larger sample from the same dataset. This is accomplished by treating different hemispheres of the brain of the same animal as repeated measurements thus acquiring a statistically more powerful sample, with a cost of losing the information about the laterality of the changes. The TBSS analysis comparing *Cstb*$^{-/-}$ mice with controls was performed at three time points (2, 4 and 6 months). Additionally, changes in FA-values over time were investigated by analysing FA-changes from 2 to 6 months inside both *Cstb*$^{-/-}$ and control groups. In order to present all TBSS results in a common 3D space, thus making comparison of affected WM-tracts easier, all 44 animals (I) were also registered into a common template brain chosen as the best registration target. The EPM1 patient data included in the translational study (II) were analysed for the laterality of the WM changes. Because of this, the data from the 6-month timepoint were treated identically to patient data and re-analysed without hemisphere mirroring.

In brief, the following TBSS protocol was used to analyse the FA-maps. First, we applied free-search of the best registration target brain from the whole data set, in order to minimize the image warping required during co-registration. The calculated best target was used in subsequent TBSS scripts as a template into which final transformations were targeted to. All brains were then co-registered to the

template brain with affine and non-linear transformations, and a mean FA-image was calculated out of all brains in the analysis. A mean FA-image was then thinned into an FA-skeleton, by thresholding the image to an FA-value 0.2, and the same step was performed to each individual FA-map. Each FA-skeleton was then projected on the mean FA-skeleton and then co-aligned with the mean FA-skeleton. AD, RD and MD parameters were also brought to the same TBSS-skeleton space using the co-registration warp-fields and tract projection information obtained in FA processing. The spatially aligned diffusion parameter data were then fed to voxelwise cross-subject statistical analysis. For all tensor parameters, null distribution in statistical testing was built up over 5000 permutations and a threshold free cluster enhancement (TFCE) method (Smith, Nichols 2009) was used to report significant findings (TFCE, $p<0.05$). In order to account for the repeated measurements in the hemisphere-mirrored data, an exchangeability block design was included in the random permutation testing.

Quantitative FA-values were extracted from FA-skeletons (**Figure 9**) on regions of interest drawn manually (aided by the significant TBSS results) along the TBSS-skeleton using a mouse brain atlas (Franklin, Paxinos 1997). Non-midline ROIs were first drawn on the left hemisphere and mirrored to the right side and corrected if there was asymmetry regarding the exact positioning of a tract in question.

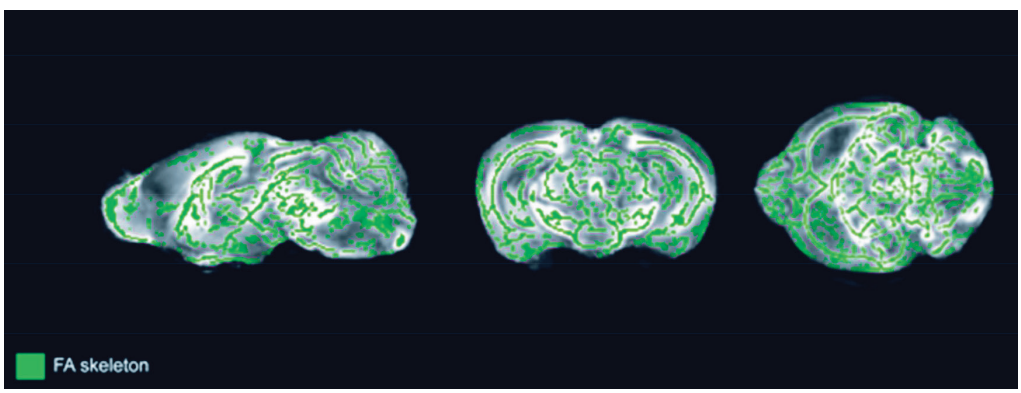

Figure 9. Co-aligning white matter tracts using a mean FA-skeleton. The mean FA-skeleton, thresholded from co-aligned FA-maps to an FA value 0.2, is shown here in green overlaied on top of the mean FA-map, calculated as mean out of all co-aligned FA-maps in the group.

3.3 WHITE MATTER HISTOPATHOLOGY (II)

3.3.1 Cerebellar myelin staining (II)

Immunohistochemical staining was performed on paraffin embedded brain slices from 6-month-old animals. The animals were anaesthetized with pentobarbital (Mebunat, 80-150 mg/kg *ip*, Orion, Finland) and perfused intracardially first with PBS with 0.16 mg/ml heparin (Sigma, St. Louis, Missouri, USA) and subsequently with pH 7.4 4% PFA. Dissected brains were immersion fixed with 4% PFA, embedded in paraffin for sectioning and cut into 5 μm sagittal sections.

The protocol for myelin basic protein (MBP) staining included quenching endogenous peroxidase activity (5% H_2O_2 in H_2O), blocking with bovine serum albumin (5% in BSA, Sigma, St. Louis, Missouri, USA) in PBS. The primary antibody was incubated overnight at +4°C (rat anti-MBP, 1:200, Chemicon, Billerica, Massachusetts, USA). For two animals (*Cstb*$^{-/-}$ n=2, both male; Control n=2, both male), immunoreactivity was detected use of biotinylated secondary antiserum IgG (1:1000; Vector Laboratories, Burlingame, California, USA) and a avidin-biotinylated peroxidase-Complex (Vectastain® Elite® ABC KIT, Vector Laboratories, Burlingame, California, USA) through reaction of diaminobenzidine tetrahydrochloride chromogen (DAB; Sigma, St. Louis, Missouri, USA). A background stain of Meyer's hematoxylin (1:2 in H_2O) was also used. For six animals (*Cstb*$^{-/-}$ n=3, control n=3, all female) immunoreactivity was detected through immunofluorecence using Alexa anti-rat secondary antibody (1:200, Invitrogen, Waltham, Massachusetts, USA). Slides were imaged using a Zeiss Axiovert 200 imaging microscope coupled with an AxioCam HRc camera and AxioVision Release 3.1 software (Carl Zeiss, Jena, Germany).

3.3.1.1 Quantification of myelin basic protein immunoreactivity (II)

Cerebellar myelin basic protein staining immunoreactivity was quantified from immunofluorescence pictures using ImageJ 1.42 (Schneider, Rasband & Eliceiri 2012). The background was subtracted with a built-in filter (**Figure 10**). The resulting image was subsequently thresholded into a binary image using a built-in movement algorithm. After this, round ROIs were placed on areas of white matter in the cerebellum by an observer blinded to the genotype of the animals (**Figure 10**). Areas of positive MBP stain were quantified as percentage of pixels over the binary threshold for positive MBP-stain.

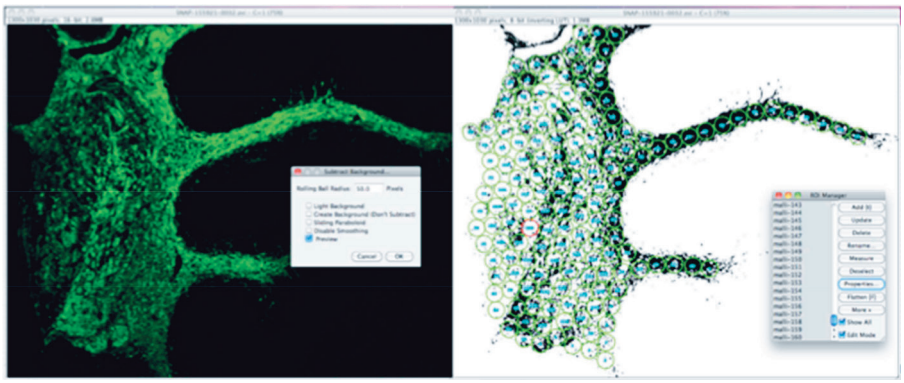

Figure 10. Quantification of cerebellar MBP-staining. The left image shows image of green MBP immunofluorescence staining of cerebellar WM after the background subtraction. The right image shows the same image as binary after thresholding, with ROIs for quantification placed on the image. The positive MBP stain was measured as a percentage of pixels (black pixels) over the binary threshold for each ROI, and a mean percentage was calculated for each image.

3.3.2 Transmission electron microscopy (II)

3.3.2.1 Sample preparation (II)

The samples for TEM were prepared from 6-month-old animals (*Cstb*$^{-/-}$ n=5, 2 male, Controls n=4, 1 male). The animals were anaesthetized with pentobarbital (Mebunat, 80-150 mg/kg *ip*, Orion, Finland) and intracardially perfused using PBS with 0.16 mg/ml heparin (Sigma, St. Louis, Missouri, USA) and perfusion fixed with 3% glutaraldehyde in 0.1 M phosphate buffer, pH 7.4. Samples from WM in the cerebellum were obtained and immersion fixed with 3% glutaraldehyde for 24h and embedded in epoxy resin.

3.3.2.2 Aquiring electronmicrographs (II)

Toludine-blue stain (1% by weight solution, Sigma, St. Louis, Missouri, USA) was used for assessing the quality of the samples, and for selecting WM regions of interest for sectioning. The blocks were subsequently sliced using an ultra microtome and stained with lead citrate and uranyl acetate. Imaging was performed using JEOL 1400 TEM (JEOL, Tokyo, Japan). From each animal, we acquired five fields with 12000x magnification (16.2 μm x 11.5 μm) of cross-sectional cerebellar WM (**Figure 11**).

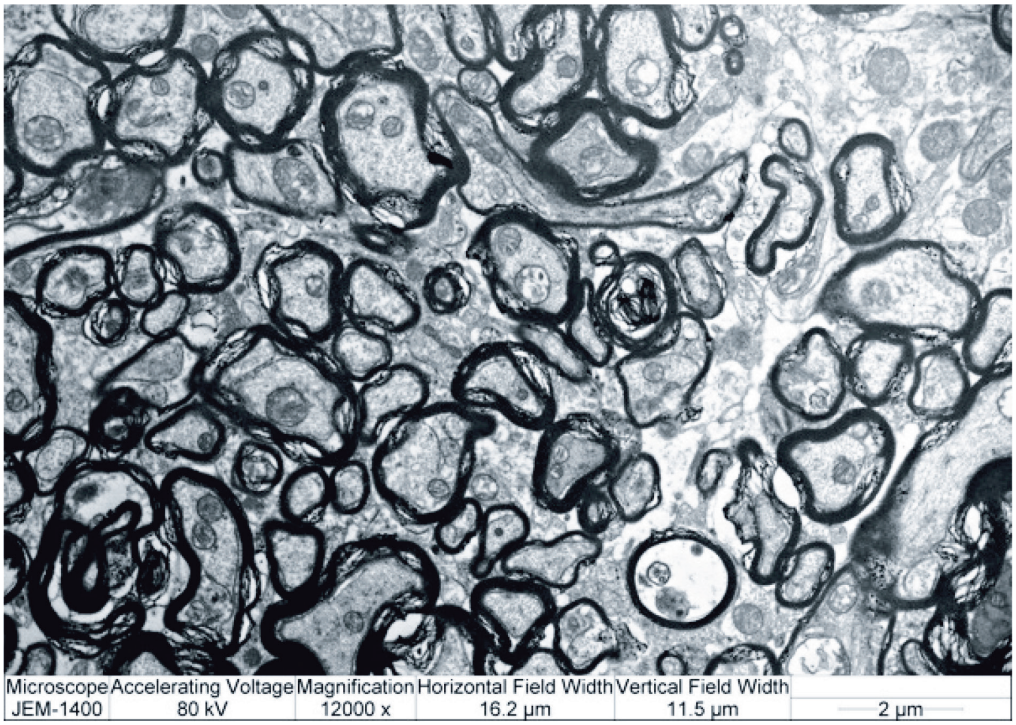

Figure 11. Transmission electron micrograph of a cerebellar white matter of a Cstb$^{-/-}$ mouse. In transmission electron microscope images, myelin sheaths of the axons can be seen as dark rings of electrondense material around the lumen of an axon. For quantification, we obtained images of cross-sectional WM with 12000x magnification.

3.3.2.3 Quantification of electronmicrographs (II)

From the electronmicrographs, we quantified axonal density and g-ratios (an index indicating the functional and structural integrity of the axon). G-ratios were quantified from ten randomly selected axons in each field (50 axons per animal) and calculated as a ratio of cross-sectional axon diameter to fibre diameter. Axonal density was quantified by counting the number of axons in the electromicrographs (5 electronmicrographs per animal) . The number of axons showing degenerative changes, including the presence of vacuolar bodies or electrondense appearance, as well as the number of degenerated axons, was calculated. Quantification was performed with ImageJ 1.42. (Schneider, Rasband & Eliceiri 2012) by a blinded observer.

3.4 BONE MICROTOMOGRAPHY (III)

3.4.1 Sample preparation (III)

For microtomography, we used 3-month-old animals (*Cstb*$^{-/-}$ n=5, all male, Controls n=4, all male). The animals were anaesthetized with pentobarbital (Mebunat, 80-150 mg/kg *ip*, Orion, Finland), intracardially perfused with phosphate buffered saline (PBS) with 0.16 mg/ml heparin (Sigma), then perfusion fixed with 4% paraformaldehyde. Hindlimbs were dissected, and post fixed for 24 h, then stored immersed in 70% EtOH.

3.4.2 Microtomography (III)

Ex vivo μCT data were acquired from the right hindlimb. During the imaging, the limbs were inserted into an in-house manufactured sealed tubular plastic imaging holder. A SkyScan 1070 μm CT scanner (SkyScan, Kontich, Belgium) was used, and the datasets were scanned with the following parameters: voxel resolution 20 μm; X-ray tube potential 70 kVp; current 200 μA; and integration time 3900 ms. The object was rotated in 0.45° steps (total 182.45°).

3.4.3 Bone morphology analysis from micrographs (III)

Cross-sectional image reconstruction was done using Nrecon 1.4 (SkyScan, Kontich, Belgium) (misalignment < 3, ring artefact reduction 11, beam hardening correction 95%, intensity gap 0.005–0.150) and analysis and modelling were performed with CTan 1.4.4 (SkyScan, Kontich, Belgium) (**Figure 12**). Cross-sectional images were binarized using an attenuation coefficient range of 0.005 to 0.150. For the trabecular bone, volumes of interest (VOI) excluding cortical bone were defined at the metaphysis of the tibia, starting 20 slices (400 μm) below the lowest identified point of the growth plate and covering 50 layers (1000 μm) downward. Analysis of cortical bone analysis was performed from the diaphysis of the tibia. VOI was defined starting 4000 μm above the growth plate, covering 100 layers (2000 μm) upward. After this, low and high threshold values for bone intensity were set to 35 and 250 respectively and the images analysed for 3D and 2D structural parameters as well as for BMD.

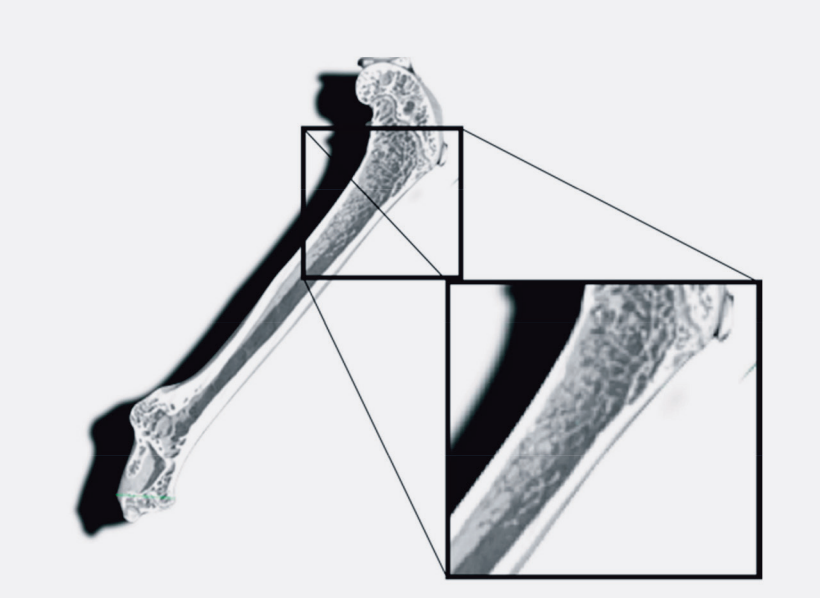

Figure 12. Computed tomography image of a control mouse femur. The high level of detail obtained by a modern computed tomography system enabled the study of porous trabecular bone structures in the mouse femur.

3.5 BONE HISTOLOGY (III)

3.5.1 Sample preparation (III)

For bone histology we prepared samples from the hindlimbs of *Cstb*$^{-/-}$ and control mice, age 1 month (*Cstb*$^{-/-}$, n=13; controls, n=13) and 4 months (*Cstb*$^{-/-}$, n=13; controls, n=13). The animals were anaesthetized with pentobarbital (Mebunat, 80-150 mg/kg *ip*, Orion, Finland), intracardially perfused with phosphate buffered saline (PBS) with 0.16 mg/ml heparin (Sigma, St. Louis, Missouri, USA), then perfusion fixed with 4% paraformaldehyde. Hindlimbs were dissected and post fixed for 24 h, then stored immersed in 70% EtOH. Histology samples were prepared from distal femurs and proximal tibias. Prior to cutting, the bones were decalcified in 5% formic acid, embedded in paraffin and cut into 5 µm-thick sections for mounting on microscopy slides. Femur length was measured using a micrometer (*Cstb*$^{-/-}$, n=5; controls, n=3) (**Figure 13**).

Figure 13. Measurement of femur length. Femur length was measured from the fixed right femur of each mouse using a micrometer.

3.5.2 Histological quantification of bone morphology (III)

Histological quantification of bone morphology was performed from hindlimb samples from 1- and 4-month-old animals (*Cstb*$^{-/-}$, n=8; controls, n=8). The cross-section of the functional zones in the growth plate (the resting-, proliferative- and hypertrophic zones) was measured as previously described (Nurmio et al. 2011). Briefly, the bone sections were stained with hematoxylin-eosin and the thickness of the zones was quantified using a Leica QWin Pro analysis system (Leica Microsystems GmbH, Wetzlar, Germany). The mature multinucleated osteoclasts were counted as previously described (Laitala-Leinonen et al. 2006) from samples stained with the leukocyte acid phosphatase kit (TRAP-kit) (Sigma Aldrich, St. Louis, Missouri, USA).

3.5.3 Immunohistological quantification of osteoclast morphology (III)

Immunohistological stainings for osteoclast cat K and tartrate-resistant acid phosphatase 5b (TRACP 5b) were quantified as described previously (Nurmio et al. 2011). In brief, stainings were done using Cat K monoclonal antibody in 1:600 dilution (Acris Antibodies GmbH, Hiddenhausen, Germany) and TRACP 5b polyconal antibody (1:500 , in-house manufacture (Halleen et al. 1998)). The number of immunopositive cells and the intensity of the staining were quantified using Leica QWin Pro analysis system (Leica Microsystems GmbH, Wetzlar, Germany).

3.6 ONE MARROW DERIVED OSTEOCLAST CULTURES (III, UNPUBLISHED)

Osteoclasts were cultured as described previously (Laitala-Leinonen et al. 2006). In brief, animals were euthanized with CO_2 and decapitated. Both femurs and tibias were harvested for bone marrow, which was then homogenized to a single cell suspension. The cell suspension was then left to adhere on 60 mm plates for 4 h in 37 °C. The non-adhered cells, which include the macrophage precursors, were washed and plated at 100 000 cells/well on 96-well plates in alpha modification of Eagle's medium (a-MEM). To promote the differentiation of the haematopoietic precursors into macrophages, the culture media included macrophage colony stimulating factor (M-CSF) 20 ng/ml (RnD systems, Minneapolis, MN, USA). Every 48 hours half of the media was replaced, and after the first 48h of culture, 100 ng/ml receptor activator of nuclear factor kappa-B ligand (RANKL, Peprotech, Offenbach, Germany) was included to facilitate osteoclast differentiation.

3.6.1 Quantification of cultured osteoclasts (III)

Osteoclasts were cultured for 6 days with RANKL, after which they were fixed with 4% PFA. Mature osteoclasts were defined as multinuclear (three or more nuclei) tartrate resistant acid phosphatase positive cells and for identifying the osteoclasts we stained the cultures using a leukocyte acid phosphatase kit (TRAP-kit, Sigma Aldrich, St. Louis, Missouri, USA). The nuclei were counterstained with Hoecst (1:500, Sigma Aldrich, St. Louis, Missouri, USA). Each well of the cultures was subsequently imaged using an Olympus ScanR system (Olympus GmbH, Hamburg, Germany), which is a modular epifluorescence microscope designed for fully automated image acquisition and analysis. The number of mature osteoclasts was counted from 22 culture wells for both genotypes (pooled from three mice per genotype in three independent experiments). The size of the osteoclasts was quantified from 9 wells for both genotypes (pooled from four mice per genotype). The number and the area of the cells was quantified by an observer blinded to the genotype of the cells using ImageJ version 1.48 (Schneider, Rasband & Eliceiri 2012).

3.6.2 Cathepsin K assay (III)

The cat K enzymatic activity assay was performed with osteoclasts cultured for 5 days on RANKL, after which the activity of cat K was assessed using Magic Red Cat K assay Kit (Immunochemistry Technologies, Bloomington, MN, USA) according to the manufacturer's instructions. Cat K present in the cultures cleaves a cresyl violet based red fluorochrome from a peptide, and the amount of produced fluorescence can

be then quantified with a plate reader. We measured the fluorescence from 8 wells for both genotypes (cells pooled from 4 mice per genotype) using a Pherastar FS plate reader (BMG Labtech, Ortenberg, Germany).

3.6.3 Osteoclast pit formation assay (III)

The resorptive capacity of osteoclasts was assayed using 96-well Corning osteo-assay surface plates (Corning, New York, NY, USA). They are cell culture plates that contain a synthetic bone coating that is digested by mature osteoclasts. Culturing and analysis were performed according to the manufacturer's recommendations, and 300000 cells/well were plated in a-MEM including M-CSF 20 ng/ml (RnD systems, Minneapolis, MN, USA) with half of the media replaced every 48 h. To facilitate differentiation of osteoclasts, after 48h 100 ng/ml RANKL was added (Peprotech, Offenbach, Germany).

The cells were cultured for 7 days with RANKL, then fixed with 4% PFA and washed with PBS. Formed resorption pits were exposed for microscopy by removing the cells with a 5 min treatment of 10% sodium hypochlorite. The formed resorption pits in the synthetic bone coating were then visualized by counterstaining the wells coating with 1% toluidine blue (Sigma, St. Louis, Missouri, USA). This makes the resorption pits discernible as clear unstained regions in the blue stained coating. The wells (*Cstb*$^{-/-}$, 10 wells; controls, 10 wells, cells pooled from 4 mice per genotype) were subsequently imaged with Olympus ScanR (Olympus GmbH, Hamburg, Germany) and a matrix of 6x8 images per well at 10x magnification was obtained. The number and the size of the pits were quantified with proprietary ScanR software version 1.3.0.3. (Olympus, Hamburg, Germany) (**Figure 14**). An edge-detection feature in the software was used for finding the edges of the resorption pits based on large image intensity difference between the dark synthetic bone and the light resorption pit. The detected pit edges were then filtered by object size for excluding false positive hits caused by well edges. Second filtering was done for a staining intensity threshold was used to exclude black staining artefacts left from the toluidine blue staining.

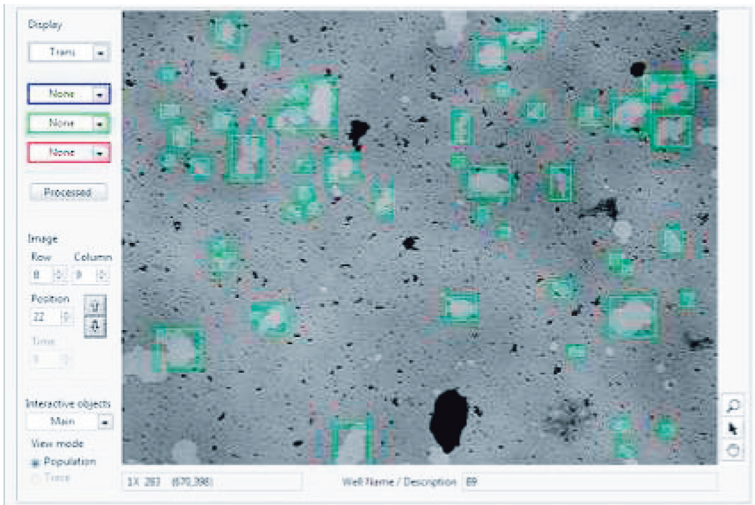

Figure 14. Number and size of formed resorption pits quantified using the ScanR software. Image shows a screen capture from program used in quantifying the resorption pit assay plates. The light resorption pits stand out on dark toluidine blue stained synthetic bone. The image shows the automated detection of resorption pit edges, with the positive hits highlighted with green squares, with almost all resorption pits detected. Black detritus seen in the image is staining artefact.

3.6.4 Fluorescence activated cell sorting (III)

The number of macrophage precursors in bone marrow was determined using fluorescence activated cell sorting (FACS). In brief, animals (3-month-old male mice, *Cstb*$^{-/-}$ n=5; control, n=3) were euthanized with CO_2 and decapitated. Bone marrow was collected from both femurs and tibias by flushing with in a-MEM using a syringe and a G23 needle. The cell suspension was homogenized to a single cell suspension in a-MEM and 1000000 cells were counted for staining. Cells were first briefly treated with a blocker (CD16/CD32, eBioscience, San Diego, California. USA) and then incubated for 30 min with an antibody cocktail for lineage exclusion (CD3e, CD11b, CD45R (B220), Ly-6G and Ly-6C (Gr-1), TER-119 (Ly-76); BD Pharmingen, San Jose, California, USA). Cells were then washed with PBS and incubated for 30 min on ice with streptavidin conjugated FITC stain and antibodies for Sca-1 and cKit (BD Pharmingen, San Jose, California, USA). After a final wash with PBS, the cells were counted with the FACScalibur system (BD Biosciences, Franklin Lakes, New Jersey, USA). The data were analysed with Flowing Software software (Flowing Software 2.5.1) (BD Biosciences, Franklin Lakes, New Jersey, USA).

3.6.5 Cell viability assay (III)

Cell viability in osteoclasts was studied using CellTiter 96® AQ_{ueous} One Solution Cell Proliferation Assay (Promega, Fitchburg, Wisconsin, USA). Osteoclasts (*Cstb*$^{-/-}$ mice n=3, all male; control mice, n=3, all male; cells pooled) were cultured for 48h, and the assay was performed according to manufacturer instructions. In brief, after administering 40 µl of the reagents to each well, the cells were incubated for 2h at 37°C. The absorbance, indicating amount of viable cells, was measured at 490 nm using a Wallac Victor2 plate reader (Perkin Elmer, Waltham, Massachusetts, USA).

3.6.6 Osteoclastic apoptosis assay (III)

Osteoclast apoptosis was assessed using TACS Blue Label TUNEL-based Apoptosis Detection Assay (R&D Biosystems, Minneapolis, Minnesota, USA). Osteoclasts (*Cstb*$^{-/-}$ mice n=3; control mice, n=3, cells pooled) were cultured 6 days on RANKL, the cells were fixed with 4% PFA and then washed with PBS. One well of control cells were treated with DNA digesting enzyme included in the kit, forming a positive control for tunel staining. The apoptosis assay was then performed for the positive control, *Cstb*$^{-/-}$ and control cells according to manufacturer instructions.

3.6.7 Quantitative real time PCR (III)

Osteoclasts (*Cstb*$^{-/-}$ mice n=3, all male; control mice, n=3, all male; cells pooled) cultured for 6 days on RANKL were analysed for gene expression changes. RNA was isolated with a Qiagen RNAeasy kit (Qiagen, Heiden, Germany) according to the manufacturer instructions. A Qiagen RT^2 Profiler PCR Array ostegenesis kit (Qiagen, Hilden, Germany) was then used to assess gene expression and Qiagen RT^2 Profiler data analysis web portal (Qiagen, Hilden, Germany) was used for determining differences in *Cstb*$^{-/-}$ osteoclast gene expression compared to that of controls.

3.7 OSTEOBLAST CULTURES (UNPUBLISHED)

Osteoblasts were cultured and characterized as described previously (Morko et al. 2009). In brief, animals were euthanized with CO_2 and decapitated. Both femurs and tibias were harvested for bone marrow, which was then homogenized to a single cell suspension. The cell suspension was then seeded into culture flasks in a density of 10^6/cm^2 and cultured for 7 days in a-MEM media with 10 mM Na-β-glycerophosphate and 50 µg/ml ascorbate-2-phosphate and with 10^{-8} M dexamethasone (Sigma, St. Louis, Missouri, USA). After 7 days of culture, the adherent cells were scraped, washed and plated at 10 000 cells/well onto 24 well plates. The cells were cultured for

another 14 days, without dexamethasone, and fixed with 4% PFA. The osteoblasts were stained for morphological analysis with with leukocyte alkaline phosphatase kit according to manufacturer instructions (Sigma, St. Louis, Missouri, USA). For assessing osteoblast function, von Kossa staining was also performed with 2% sodium nitrate and 2.5% sodium thiosulfate solutions (Sigma, St. Louis, Missouri, USA).

3.8 STATISTICAL ANALYSIS (I, II, III, UNPUBLISHED)

The statistical analysis of data was done using one- and two-way analysis of variance (ANOVA), with Bonferroni correction used where applicable. The statistical analysis was performed with Microsoft Excel for Mac 2011 (Microsoft, Redmond, Washingon, USA) and GraphPad Prism 5.0c software (GraphPad Software, San Diego, California, USA), with P-values smaller than 0.05 considered significant. Statistical methods for the TBSS-analysis (I,II) have been detailed in their corresponding methods sections (3.2.2.3).

4 RESULTS AND DISCUSSION

4.1 WHITE MATTER DEGENERATION AND ATROPHY IN *CSTB*$^{-/-}$ MICE (I,II, UNPUBLISHED)

4.1.1 Early and widespread atrophy in Cstb$^{-/-}$ mice (I)

Previous imaging studies have reported cerebellar, thalamic and cortical atrophy in EPM1 patients (Mascalchi et al. 2002, Koskenkorva et al. 2009). Correspondingly, the brain volume in adult patients has been shown to be decreased by 10% compared to healthy controls (Koskenkorva et al. 2009). The limited histopathological data on EPM1 patients has shown loss of cerebellar granule and Purkinje cells as well as neuronal degeneration and neuronal loss in the cerebral cortex, striatum, thalamus and brain stem (Cohen et al. 2011, Eldridge et al. 1983, Haltia, Kristensson & Sourander 1969, Koskiniemi et al. 1974). Even though the progressive nature of atrophy in EPM1 has been difficult to demonstrate, the severity of myoclonus has been associated with cortical thinning (Koskenkorva et al. 2009). The histopathological findings in the *Cstb*$^{-/-}$ mice are very similar to those in EPM1 patients, although atrophy is more severe in the *Cstb*$^{-/-}$ mouse brain (Shannon et al. 2002, Tegelberg et al. 2012). In order to elucidate the progress and the spatiotemporal dynamics of the atrophy, a longitudinal *in vivo* MRI volumetry study in *Cstb*$^{-/-}$ mice was carried out. The time points for the study were selected to correspond with our previous histology study (Tegelberg et al. 2012) and the manifestation of disease symptoms in the mouse model: the first signs of myoclonus manifest at 1 month of age, and by 6 months of age the animals develop ataxia and become fully symptomatic (Pennacchio et al. 1998).

The MRI volumetry revealed the whole brain volume, excluding the medulla, to be significantly reduced in *Cstb*$^{-/-}$ mice compared to controls already at 1 month (**I, Figure 1 A**). Whereas the whole brain volume in controls increased until 4 months, in *Cstb*$^{-/-}$ mice the atrophy overtook the growth and the brain volume decreased from 2 months onwards (**I, Figure 1 A**), highlighting the severity of the atrophy and suggesting that the brain size never reaches that of the controls. No difference in cerebellar volume between controls and *Cstb*$^{-/-}$ mice was observed at 1 month, but from at 2 months onwards, the cerebelli of *Cstb*$^{-/-}$ mice were significantly smaller (**I, Figure 1 B**). In control mice the cerebellum continued to grow in size until 2-month timepoint, whereas in *Cstb*$^{-/-}$ mice, the cerebellar volume progressively decreased from 1 month onwards (**I, Figure 1 B**). Progression of the volume loss in the cerebral cortex (**I, Figure 1 C**) was similar, with *Cstb*$^{-/-}$ mice showing a significant decrease from 2 months onwards. On the contrary, the striatum and the hippocampus (**I, Figure 1 D and E**) showed significant reduction in volume only at 6 months of age.

The data show that the atrophy has an early onset and is progressive. The difference in volume between the groups was accentuated over the observation period as the volume in the control group continued to grow whilst the brain volume decreased in the *Cstb*$^{-/-}$ group, emphasising the progressive nature of the atrophy. Furthermore, the heterogeneity in the degree and rate of volume loss in different brain regions would indicate that some cell populations are more sensitive to the lack of CSTB than others. Still, even though we did not detect statistically significant atrophy of individual brain regions at the 1-month time point, the cumulative volume loss from individual regions added up to a significantly decreased whole brain volume at this point. As *Cstb*$^{-/-}$ mice show signs of neuroinflammation and microglial activation already at age of p14 (Okuneva et al. 2015, Tegelberg et al. 2012) and neuronloss at 1 month (Tegelberg et al. 2012), the severe and early atrophy shown here emphasises the presence of early changes in EPM1, and suggest that that disturbed developmental processes constitute to the observed changes.

4.1.2 Widespread and progressive FA decrease in the Cstb$^{-/-}$ mice (I)

In agreement with the findings of progressive atrophy demonstrated by the results, loss of neuronal volume in the posterior fossa in EPM1 patients has been reported (Mascalchi et al. 2002) and a recent VBM study showed GM volume loss in bilateral cortical motor areas and thalami (Koskenkorva et al. 2009). The atrophy in the motor cortex matched the results of a navigated transcranial magnetic stimulation (TMS) study, which could be indicated in cortical inhibitory networks (Danner et al. 2009). Myoclonus, the pathophysiological basis of which is currently not yet well understood, is the most disabling symptom in EPM1 and therefore it can be assumed that motor pathways are widely affected. The findings from our previous histology study (Tegelberg et al. 2012) as well the drastic and early cortical atrophy (I) support this hypothesis, even though a previous histology study showed no indication of myelin changes beyond WM gliosis (Shannon et al. 2002). The presence WM changes in *Cstb*$^{-/-}$ mice were investigated using DTI and the obtained data analysed with TBSS. No previous MRI data from the mouse model existed, and histopathological data from *Cstb*$^{-/-}$ mice were scarce, making a hypothesis-based ROI selection with manual quantification of DTI data an unfeasible approach. Also, the previously described (4.1.1) prominent atrophy could hinder the ROI selection and further encouraged the use of an automated approach. The study period for the experiment was selected to complement the *in vivo* volumetry (4.1.1) with 2, 4 and 6 months time points analysed.

Ex vivo FA TBSS analysis of the DTI data revealed significant decrease in FA compared to the controls already at the 2 months timepoint (**I, Figure 2 A; blue colour**). The FA decrease was observed on several brain regions, including the

cerebellum, cerebral cortex, external/internal capsule, hippocampus, hypothalamus, and thalamus, with the most severe changes in the cerebellum and the thalamus **(I, Table 1)**. These results highlight the drastic nature of the cerebellar and thalamic changes and early onset of WM changes, as indicated by FA decrease. By 4 months of age, more widespread areas of decreased FA within the cerebellum, cerebral cortex, external/internal capsule, hippocampus, hypothalamus, and the thalamus were observed (**I, Figure 2 A; yellow colour**). Furthermore, many brain regions not shown affected by the TBSS at 2 months, including the corpus callosum, medulla, and the striatum, were showing significant decrease in FA by 4 months (**I, Figure 2 A; yellow colour**). The new affected areas that emerge over time emphasise the progressive nature the changes. At 6 months, the decrease in FA was seen extending on larger areas on the previously affected brain regions and spreading most notably in the cerebellum, corpus callosum, hypothalamus and thalamus **(I, Figure 2 A; red colour).** Contrary to other regions, at 6 months of age, only minor changes were observed in the hippocampus. The TBSS analysis also showed significantly higher RD in the thalamus and the cerebellum of the *Cstb*$^{-/-}$ group at 4 months and in the cerebellum at 6 months (**Unpublished, Figure 15; I, Table 1**). As no changes in AD or MD were observed, it is likely that increase in RD contributes the most to the observed decrease in FA, at least at the timepoints of 4 and 6 months. Like the observed atrophic changes, the FA decrease was progressive and spatiotemporally heterogeneous. Based on these findings, the sequence of the pathological events in the *Cstb*$^{-/-}$ mice has been detailed in Figure 3 (**I, Figure 3**). The order and timing of the observed changes indicate that the early-onset non-uniform microglial activation, astroglial activation, neuron loss, myoclonus (Pennacchio et al. 1998, Tegelberg et al. 2012) and the atrophy shown in 4.1.1 precedes the observed the FA decrease. Thus the cascade of previous neurodegenerative events would indicate that the WM changes suggested by the FA decrease are most likely a secondary phenomenon to the preceding pathological changes and not as such directly caused by the lack of CSTB.

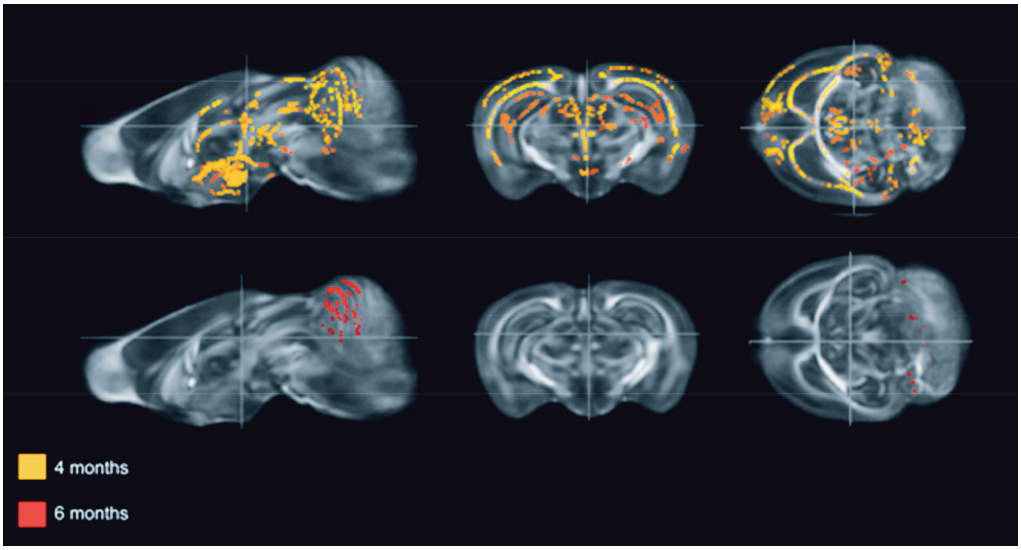

Figure 15. Areas of increased RD in 4- and 6-month-old Cstb$^{-/-}$ mice. Areas of significantly increased RD (TFCE p<0.05, corrected for multiple comparisons) in 6-month-old ***Cstb***$^{-/-}$ mice (red) and in 4-month-old ***Cstb***$^{-/-}$ mice (yellow) overlaid on a mean FA image of the study population. Both exhibit changes in the cerebellum, with significant changes seen on also other areas, including the thalamus, in the 4-month-old group. This is likely due to the larger amount of analysed brains in the 4 month group. No areas of decreased RD were observed.

4.1.3 On-going pathological processes hinder WM maturation in the *Cstb*$^{-/-}$ mice (I)

A longitudinal TBSS analysis was also performed for *Cstb*$^{-/-}$ and control groups, comparing the changes in FA from 2 to 6 months in each group. The results of this analysis showed that FA in the WM changed as the animals aged and the WM matured (**I, Figure 2 B; I, Table 1**). TBSS analysis in the control group revealed that the FA-values in most WM tracts at 2 months were significantly lower when compared to values at 6 months (**I, Figure 2 B, pink colour**), demonstrating FA increase in the WM as the animals age. In line with the results, previous studies have reported FA increase over time in healthy mice, and this is thought to reflect the maturation of the WM as the reorganization and compaction leads to increased fibre tract coherence (Larvaron et al. 2007, Chahboune et al. 2007). In concordance with our findings, these processes have been demonstrated to continue well beyond 2 months of age (Verma et al. 2005). Similar FA increase was also observed in the *Cstb*$^{-/-}$ group (**I, Figure 2 B, green colour**), although the FA increase was detected in fewer brain regions. Also, on some brain regions such as the hypothalamus, thalamus and cerebellum, the changes were detected only in restricted sub-regions. The less pronounced FA increase over time therefore is likely to reflect the underlying

degenerative changes that hinder the WM maturation.

We had previously performed TBSS analysis of DTI data in another mouse model of a neurodegenerative disease, ceroid lipofuscinosis type 8 (CLN8). While the animals displayed WM-changes in form of delayed myelination (Kuronen et al. 2012), TBSS was not able to discern this defect (unpublished results), demonstrating that even drastic WM changes that do not cause changes in FA remain undetected with TBSS. However, in addition to a previously reported investigation on the WM changes in the mouse model of the Pelizaeus-Merzbacher disease[114], the studies reported in this thesis (I, II) are among the first demonstrating the use of TBSS in investigating neurodegenerative changes in mice. Furthermore, longitudinal TBSS-studies have previously only been performed in patients (Poudel et al. 2015, Madhyastha et al. 2014), and these results introduce the use of TBSS in the study of progressive WM changes in animal models of neurodegeneration. The findings also show the feasibility of longitudinal TBSS as a tool for following FA changes related to normal WM maturation and reorganisation.

4.1.4 Axonal degeneration in *Cstb*$^{-/-}$ mice (II)

Since the decreased FA (I) suggested progressive WM changes in the brain of the *Cstb*$^{-/-}$ mice, immunohistochemical analysis was performed in order to link DTI findings to tissue level changes. The longitudinal FA TBSS (**I, Figure 2 A; Table 1**) indicated the cerebellum as the most severely affected brain region with early onset of damage. Combined with the previous histological data available from the region (Tegelberg et al. 2012, Shannon et al. 2002), the histological investigation of WM changes was conducted from of 6 month old *Cstb*$^{-/-}$ mice, with quantitative analysis performed on the cerebellum.

The immunohistochemical staining of MBP showed decreased immunoreactivity in the brain of *Cstb*$^{-/-}$ mice, most notably in the cerebellum (**II, Figure 2 A, B)** and quantification of the immunoreactivity revealed significant ($p=0.027$) decrease in MBP staining intensity in the *Cstb*$^{-/-}$ mice. Immunohistochemistry results indicated demyelination as the most likely cause of the FA decrease. Thus myelination was studied by using TEM images for determining axonal g-ratios, an established index describing axonal myelination (Chomiak, Hu 2009). As the quantification of g-ratios from TEM images did not indicate any difference in axon myelination between *Cstb*$^{-/-}$ mice and controls (g-ratios: *Cstb*$^{-/-}$ 0.71±0.01 vs. Control 0.69±0.02), it seemed unlikely that the changes in axon myelination cause the observed FA decrease. Therefore changes in axonal density were studied as a possible source for decreased MBP-immunoreactivity. This revealed a tendency toward lower axonal number in the *Cstb*$^{-/-}$ animals (*Cstb*$^{-/-}$ 38±7 vs. control 56±9 per field; $p=0.065$). As the electromicrographs of *Cstb*$^{-/-}$ mice exhibited an unusual amount of dead and

degenerating axons, we continued to investigate axonal degeneration. This revealed significantly more dead and degenerating axons (*Cstb*$^{-/-}$ 2.09±0.29 vs. control 0.48±0.19 per field, p=0.002) in the cerebellar WM of the *Cstb*$^{-/-}$ animals. The high number of degenerating axons, combined with the lower axonal density indicated a drastically higher amount of axon damage in *Cstb*$^{-/-}$ mice compared to the controls. *Cstb*$^{-/-}$ animals had one axon showing degenerative changes in one for every 19 healthy axons, whereas controls had the ratio of one in 117 (**II,Figure 3 A,-C**).

In light of these results, it appears that the axonal degeneration with consequent loss of whole fibres leads to a higher extracellular volume in the WM. As increased axonal spacing subsequent to axon loss has previously been associated with an increase in RD (Sen, Basser 2005), it is likely that the larger extracellular volume subsequently leads to an increase in RD, corresponding with the changes observed in the cerebellum at 4 and 6 months (**Unpublished**, **Figure 15**), the most severely affected brain region. The increase in RD in turn translates into decrease in FA. Therefore it is likely that the WM tracts exhibiting decreased FA are undergoing local axon loss matching the one demonstrated in the cerebellum of the *Cstb*$^{-/-}$ mice. The results also highlight FA as a more robust indicator of WM damage, since FA TBSS is able to show significant changes on most major WM tracts compared to the limited changes illustrated by the RD TBSS.

4.1.5 White matter degeneration in EPM1 is caused by axon loss (II, Unpublished)

The correspondence of WM changes present in EPM1 patients and *Cstb*$^{-/-}$ mice was investigated in a translational setting. A TBSS-analysis of the DTI data comparing adult EPM1 patients and healthy controls (II) was performed without hemisphere mirroring, since this facilitated the study of the laterality of the changes between the hemispheres. The approach was matched in the animal model by comparing the DTI data from the fully symptomatic 6-month-old *Cstb*$^{-/-}$ mice with controls in a new analysis without the hemisphere mirroring. The TBSS analysis of DTI data revealed the WM of EPM1 patients to be widely affected. The degree and the widespread nature of the damage was highlighted by the global FA decrease along the TBSS skeleton (II). The *Cstb*$^{-/-}$ mice revealed corresponding changes with a significantly decreased global FA over the TBSS skeleton (*Cstb*$^{-/-}$ 0.397± 0.0018 vs. control 0.415 ± 0.0057, Student's t-test p=0.022). The TBSS-analysis showed significantly decreased FA on almost all major WM tracts of EPM1 patients, with parallel changes in more limited brain regions observed in the *Cstb*$^{-/-}$ mice (**II, Figure 1 A, B; Table 3E**).

TBSS revealed previously overlooked affected brain regions both in EPM1 patients

and *Cstb*$^{-/-}$ mice, the most notable of these being the changes in the cerebellum in patients and in the thalamus in *Cstb*$^{-/-}$ mice. Cerebellar changes in some autopsied EPM1 patients have been previously reported, but these have been attributed to phenytoin treatment (Eldridge et al. 1983). While a recent histopathological study showed cerebellar changes in an EPM1 patient with no history of phenytoin treatment[51], the discrepancy between extensive cerebellar changes in the *Cstb*$^{-/-}$ mice (Tegelberg et al. 2012, Pennacchio et al. 1998, Shannon et al. 2002) and the minor changes in patients have been attributed to differences in pathologies between the species. As DTI revealed cerebellar changes in both the EPM1 patients and the adult mouse model of the disease, our data suggest that cerebellar changes are a common characteristic of the disease. Due to the cerebellar role in movement coordination, it is also possible that these changes contribute to the ataxia present in the disease. Furthermore, a VBM study in EPM1 patients showed grey matter volume loss in the thalamus (Koskenkorva et al. 2009) and histological analysis has indicated the thalamus to be affected in EPM1 patients (Koskiniemi et al. 1974). Before a recent report by our group about microglial activation, followed by astrocytosis and neuron loss in the thalamocortical system of *Cstb*$^{-/-}$ mice (Tegelberg et al. 2012), there were no reports of the thalamus being affected in *Cstb*$^{-/-}$ mice. Taken together with the current data, the findings emphasize the involvement of the thalamus in the pathogenesis of EPM1 and the discovery of previously overlooked affected areas highlight the benefits of the use of the hypothesis free approach of TBSS.

In EPM1 patients, the majority of voxels with decreased FA corresponded to increased RD and MD while AD was unchanged (II). In patients and in mice, both hemispheres showed equivalent FA changes, indicating that WM damage displays no laterality. TBSS comparison between the *Cstb*$^{-/-}$ group and the controls did not show significant decrease in AD, MD or RD. However, the TBSS revealed the *Cstb*$^{-/-}$ group to have significant increase (TFCE $p<0.05$ with multiple comparison correction) in cerebellar RD (**Unpublished, Figure 16**). As a whole, increased RD (and to some degree, MD) would appear to be the main contributors to the FA decrease in EPM1 patients and *Cstb*$^{-/-}$ mice. The TEM results indicated that the underlying cause of these changes is axonal degeneration. Decreased FA together with increased RD and MD coinciding with axonal death has been reported in patients with amyotrophic lateral sclerosis (Cosottini et al. 2005), corpus callosotomy (Concha et al. 2006), and traumatic WM injury (Sidaros et al. 2008). The changes seen in the brains of EPM1 patients follow a pattern of chronic WM degeneration, reflecting both myelin and axonal loss (Concha et al. 2006, Sun et al. 2008, Burzynska et al. 2010). Thus it is likely that the brain structures that display lowered FA in EPM1 patients are undergoing a local pathology similar to that illustrated in *Cstb*$^{-/-}$ mice. The treatment resistant myoclonus has been previously considered predominantly cortical in nature (Kälviäinen et al. 2008, Koskenkorva et al. 2009). Altered inhibition in the

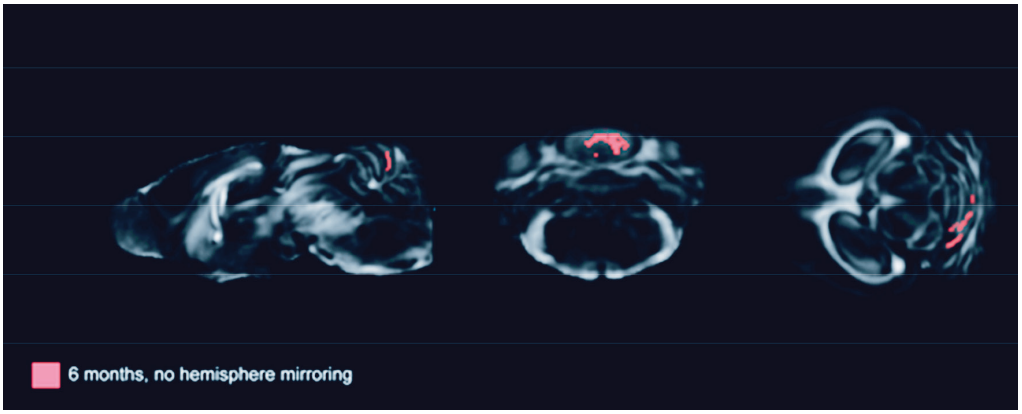

Figure 16. TBSS comparison of RD between 6-month-old Cstb$^{-/-}$ mice and controls without hemisphere mirroring shows increased RD in the cerebellum. Areas of significantly increased RD (TFCE π<0.05, corrected for multiple comparisons) are shown in red overlaid on a mean FA image of the study population, and show elevated RD in the cerebellum of *Cstb*$^{-/-}$ mice. The results show some laterality in the changes, and when compared with the changes with hemisphere mirroring, demonstrate that more significant changes can be observed due to the more robust statistical processing. No areas of decreased RD were observed.

thalamocortical system of the patients has previously been demonstrated (Mervaala et al. 1984, Mervaala et al. 1986), and a thalamocortical dopaminergic defect has been reported (Korja et al. 2007b). The TBSS results indicate that in EPM1 there are widespread WM alterations including the subcortical WM, the pyramidal tracts and thalamus that parallel previously reported GM volume loss in the motor cortex and thalamus (Koskenkorva et al. 2009). Both the cerebellum and thalamus are linked to motor function (Manto et al. 2012, Sommer 2003), and the early manifestation of both the atrophy and WM changes at these regions combined with the coinciding emergence of myoclonus at one month of age emphasize thalamic and cerebellar involvement in the myoclonus. Therefore it is likely that the motor disturbances in EPM1, myoclonus included, are not only cortical in nature but also involve the thalamocortical system and are augmented by the impaired inhibition and movement control by the damaged cerebellum. Furthermore, the novel information about the disease progress suggest that possible therapies in EPM1 should be targeted to the early stages of the disease, as the atrophy and WM damage are irreversible and are likely to contribute to the severe treatment resistant myoclonus in patients.

Research of the mouse model of multiple sclerosis has shown microglial cathepsin K, which is inhibited by CSTB, to contribute to the WM damage present in the disease (Ma et al. 2007). Moreover, the mice deficient in CSTB and cathepsin B undergo less severe cerebellar atrophy and the cathepsin B levels are known to be increased in cells of both the EPM1 patients and the *Cstb*$^{-/-}$ mice (Houseweart et

al. 2003, Lehtinen et al. 2009, Rinne et al. 2002). Findings in Alzheimer's disease, Parkinson's disease, amylotropic lateral sclerosis and Huntington's disease also show activation of microglia and the secretion of pro-inflammatory cytokines to play a role in the pathogenesis (Prinz, Mildner 2011). Therefore, elevated cathepsin B levels combined with deficient inhibitive function of CSTB could contribute following WM loss.

4.2 BONE PHENOTYPE IN *CSTB*$^{-/-}$ MICE (III)

4.2.1 CSTB deficiency affects bone structure and osteoclast homeostasis (III)

In addition to the widely documented neurological features, EPM1 patients exhibit heterogeneous bone changes, including diffuse thickening of cranial bones, arachnodactyly, scoliosis, enlarged paranasal sinuses, and accessory ossicles of the foot (Danner et al. 2013, Korja et al. 2007a, Suoranta et al. 2012). The cause and origin of these bone changes is currently unknown and the bone phenotype of *Cstb*$^{-/-}$ mice had not been characterised before. Therefore it was justified to investigate whether the bone phenotype is recapitulated in *Cstb*$^{-/-}$ mice and examine the function of CSTB in bone metabolism and especially osteoclasts using the *Cstb*$^{-/-}$ mouse model.

The bone structure in hindlimbs of *Cstb*$^{-/-}$ mice was studied with μCT. The analysis of the cortical BMD did not show any change (*Cstb*$^{-/-}$ 0.208±0.01 vs. control 0.189±0.06), while the trabecular BMD was significantly higher in the *Cstb*$^{-/-}$ mice (0.339±0.02 vs. controls 0.243±0.01, T-test p=0.001). Analysis of the three-dimensional bone structure from the μCT data revealed changes in trabecular bone composition (**III, Table 1**), most importantly increased trabecular thickness and increased bone volume percent (bone volume / tissue volume). The diffuse thickening of the skull in EPM1 patients is known also to affect the trabecular bone (Suoranta et al. 2012, Korja et al. 2007a). While no data on BMD measurements from EPM1 patients exist, the osteoporotic changes reported in trabecular bone (Suoranta et al. 2012) could indicate decreased BMD.

These findings indicate that the lack of CSTB in the mouse model leads to altered formation of bone tissue especially in the trabecular bone, as would be expected based on the changes observed in the trabecular bone of patients. Other bone abnormalities reported in EPM1 patients, e.g. scoliosis, arachnodactyly and accessory ossicles of the foot, are linked to skeletal growth (Suoranta et al. 2012). While no macroscopic morphological bone changes were identified in *Cstb*$^{-/-}$ mice, analysis of growthplate thickness from fixed and then decalcified hind limb sections revealed the growth plates in both the distal femurs and proximal tibias of the *Cstb*$^{-/-}$ mice to be significantly thinner compared to controls. The difference was observed both at the 1 and 4 months

timepoints (**III, Figure 1**). Still, even though *Cstb*$^{-/-}$ mice have been reported to weight less than healthy controls (Shannon et al. 2002), no difference in the length of the femur was observed (*Cstb*$^{-/-}$ 15.7 mm ± 0.17 vs. control 16.13 ±0.16, p=0.064).

Possible causes for the observed changes in bone morphology were investigated in more detail from histological data. Counting the number of osteoclasts from sections of fixed and decalcified hind limb bone tissue revealed significantly decreased numbers of osteoclasts in *Cstb*$^{-/-}$ mice compared to controls. This difference was observed both at 1-and 4-months of age, in both the distal femurs and proximal tibias (**III, Figure 2**). Evaluation of the resorptive capacity of the osteoclast was done by quantifying immunohistochemical staining for TRACP 5b and cat K. This revealed higher expression of both TRACP 5b and sat K in the osteoclasts of *Cstb*$^{-/-}$ mice, suggesting higher resorptive capacity per cell (**III, Figure 2**). As osteoblast cultures from *Cstb*$^{-/-}$ mice showed no indication of changes in cell morphology or function when compared to controls (data not shown), the findings imply that a reduced number of osteoclasts with possibly increased resorptive capacity are likely to contribute to the bone morphology changes associated with CSTB deficiency. The contribution of secondary factors to the observed skeletal changes in EPM1 patients has been previously discussed. Antiepileptic drugs, especially phenytoin, are known to cause calvarial thickening (Kattan 1970) and have previously been speculated to contribute to the bone changes in the EPM1 patients (Suoranta et al. 2012). Due to severe myoclonus, some EPM1 patients are also wheelchair bound. As immobility is known to affect bone structure and composition (Cervinka et al. 2011), the possible contribution of reduced mobility on bone findings in EPM1 patients has also been discussed (Suoranta et al. 2012). Nevertheless, the *Cstb*$^{-/-}$ mice showed changes in both trabecular bone structure and composition before the manifestation of ataxia at 6 months, so it is unlikely that immobility would contribute to the observed bone changes. The mice are also not subjected to any antiepileptic therapies and therefore the findings indicate that the bone changes in EPM1 patients are a direct result of deficient CSTB function resulting from changes in skeletal remodelling. Since skeletal changes do not appear to be a secondary phenomenon, they do not as such warrant changes in patient care e.g. modifying anti-epileptic medication.

4.2.2 Impaired bone resorption in bone marrow derived *Cstb*$^{-/}$ osteoclast cultures (III)

The findings from histology indicated that changes in osteoclast homeostasis could be responsible for the bone phenotype in *Cstb*$^{-/-}$ mice. The results suggest that changes in progenitor cell populations, cell viability, or apoptotic cell death of the osteoclasts may contribute to the observed bone changes. The possible changes in osteoclast function and homeostasis were therefore explored further in bone marrow

derived osteoclast cultures. Quantification of the cultures revealed a lower number of mature TRAP-positive multinucleated osteoclasts in the *Cstb*$^{-/-}$ cultures and the osteoclasts were also smaller compared to controls (**III, Figure 3**). Since both bone histology and osteoclast cultures indicated decreases in osteoclast numbers in *Cstb*$^{-/-}$ mice, the possible causes for this were investigated. First, a colorimetric assay was performed to study cell viability in the cultures, but no significant differences between the genotypes were observed (*Cstb*$^{-/-}$ 0.335 ± 0.007 absorbance units vs. control 0.328 ± 0.006 absorbance units; p=0.12), indicating that the viability of *Cstb*$^{-/-}$ osteoclasts is not compromised.

Next, the possible changes in precursor cell populations that could contribute to the observed osteoclast phenotype were investigated. Our previous studies have shown that the *Cstb*$^{-/-}$ mice exhibit early and severe microglial phenotype with microglial activation already at age P14 and increased chemokine release and chemotactic activity at P30 (Tegelberg et al. 2012, Okuneva et al. 2015). As microglia and osteoclasts share a common macrophage progenitor cell lineage, and multinuclear mature osteoclasts form through fusion of pre-osteoclastic cells, differences in macrophage progenitor population could translate into a smaller number of mature osteoclasts. Therefore possible changes in the composition of the progenitor cell population were investigated by performing flow cytometric analysis on bone marrow composition. The changes in the progenitor pool are however an unlikely cause for the decrease in osteoclast numbers since the number of macrophage precursors was actually slightly higher in the *Cstb*$^{-/-}$ mice (*Cstb*$^{-/-}$ 395 ± 56 cells per 100000 counted vs. control 247 ± 46 cells per 100000 counted; p=0.03).

Third, we investigated the possible contribution of apoptotic cell death to the observed decrease in *Cstb*$^{-/-}$ osteoclast numbers. CSTB has been previously demonstrated to be capable of inhibiting osteoclast apoptosis and regulating bone resorption *in vitro* (Laitala-Leinonen et al. 2006). Furthermore, cathepsin K, which cystatin B inhibits has been shown to act as a modulator of osteoclastic apoptosis and senescence (Wilson et al. 2009, Chen et al. 2007). Therefore, cat K mediated osteoclastic apoptosis was investigated as a cause for the decrease in osteoclast numbers. Nonetheless, TUNEL staining did not show indications of apoptotic cell death in the cultures (**III supplement, Figure 1**).

As the results would suggest that changes in progenitor cell numbers, cell viability or apoptotic cell death were not likely to contribute to the observed changes in osteoclast numbers, a qPCR-based gene expression profiling was performed from osteoclast cultures in order to determine if changes in the gene expression could implicate possible causes for the decrease in osteoclast numbers. The results of qPCR-array illustrated moderate changes in genes related to cell growth, differentiation and resorptive function (**III, Table 2, supplement Table 1**). However, none of these

as such provided a direct explanation to the change in *Cstb*$^{-/-}$ osteoclast numbers. Bone morphogenic proteins (BMP) are a group of proteins known to promote osteoclast survival and differentiation (Okamoto et al. 2006, Wutzl et al. 2006, Itoh et al. 2001). In the array, BMPs were shown to be downregulated in the *Cstb*$^{-/-}$ osteoclasts, with BMP3 downregulated 8-fold. Furthermore, activin A receptor 1, which relays the signals from BMPs and is known to have an important role in osteoclast differentiation (Fuller, Bayley & Chambers 2000), was also downregulated 1.5-fold. Genes connected with the resorptive function of the osteoclasts, such as matrix metallopeptidase 9 (MMP9), a protein playing an important role in bone remodelling (Ortega et al. 2003), was upregulated 4-fold and cat K 1.9-fold, the changes possibly reflecting compensatory mechanism in resorptive function due to smaller osteoclast numbers. Whether these changes simply reflect the phenotype of the osteoclast cultures, or are actually underlying causes responsible for the bone changes observed in the *Cstb*$^{-/-}$ mice, and probably in patients, remains unclear.

Both the changes in gene expression and the quantification of staining intensity for TRACP 5b and cat K suggested elevated resorptive capacity in individual *Cstb*$^{-/-}$ osteoclasts. A fluorescence based cat K assay was subsequently performed in osteoclast cultures but contrary to this hypothesis, the enzyme activity per well did not significantly differ between genotypes (*Cstb*$^{-/-}$ 0.97 vs. Control 1.00 fluorescence units). While *in vitro* results show no indication of elevated cat K activity, based on gene expression and immunohistochemistry data, enzymatic capacity for resorption in individual *Cstb*$^{-/-}$ osteoclasts might in fact be elevated compared to the controls, especially as CSTB has previously been shown to suppress osteoclastic resorption *in vitro* (Laitala-Leinonen et al. 2006).

We subsequently investigated whether the resorption capacity of *Cstb*$^{-/-}$ osteoclasts was indeed elevated compared to controls. The resorptive capacity was studied *in vitro,* by culturing osteoclasts in wells with synthetic bone coating. The experiment revealed that both the number and the area of the formed resorption pits was significantly decreased in the *Cstb*$^{-/-}$ osteoclast cultures (**III, Figure 4)**. The results therefore suggest that even though the enzymatic resorptive capacity of the individual osteoclasts appears to be elevated, the overall resorptive capacity in the cultures is severely compromised, at least *in vitro*. The resorptive capacity is closely connected to both the cell number and cell size (Xing, Xiu & Boyce 2012). The lower overall resorption suggests that the higher resorptive capacity per cell is not able to overcome the effect of lower osteoclast number and size in the *Cstb*$^{-/-}$ group. It is also likely that the observed higher resorptive capacity per cell is, at least to some degree, a compensatory mechanism to the decrease in resorptive function.

As resorption pit formation assay revealed decreased resorptive capacity in the *Cstb*$^{-/-}$ cultures, it is likely that the thicker trabeculae and more heavily mineralized

bone in *Cstb*$^{-/-}$ mice are an outcome of the deficient resorptive function caused by the decreased osteoclast number and size. Since the bone findings seen in patients are not likely to result from reduced mobility or anti-epileptic therapies, it is probable that the bone changes present in EPM1 are caused by changes in osteoclast function and homeostasis, parallel to the changes demonstrated in *Cstb*$^{-/-}$ mice. While the exact mechanism by which a lack of CSTB leads to the changes in osteoclast homeostasis remains undisclosed, the current results indicate the role of CSTB in bone goes well beyond cat K inhibition, a view supported by previous studies (Laitala-Leinonen et al. 2006). Furthermore, cells cultured from cat K deficient mice with 129/Sv background have been shown to lack normal apoptosis and cellular senescence, and in a pre-osteoclastic cell line, induced cat K expression led to premature cellular senescence (Chen et al. 2007). Therefore the contribution of premature, possibly cat K mediated, cellular senescence to observed changes in osteoclast homeostasis and function should be further investigated.

5 CONCLUSIONS

This thesis examined the progress and the background of the pathological changes in EPM1 in the brain and bone by utilizing advanced imaging methods and modern image analysis methodology in the mouse model of the disease. The *in vivo* MRI volumetry in *Cstb*$^{-/-}$ mice exposed spatiotemporally heterogeneous atrophy in that was demonstrated to be progressive and the findings in a longitudinal TBSS analysis revealed widespread and progressing WM damage with parallel development. As the TBSS results demonstrated high correspondence between the findings in the *Cstb*$^{-/-}$ mice and EPM1 patients, this suggested that patients also undergo similar axonal degeneration as demonstrated in the mouse model of the disease. The results showed disturbed thalamocortical connections and cerebellar damage that is likely to contribute to the observed disabling motor disturbances in EPM1. The extent of this damage also gives an indication of why the myoclonus in EPM1 remains resistant to treatment. The spatiotemporal order of subsequent pathological changes demonstrated in this study suggests that the WM pathologies in EPM1 could be secondary in the disease process, and thus possibly be avoided with early therapeutic interventions. Therefore future investigation must be aimed at the first stages of disease. As the earliest observed changes in *Cstb*$^{-/-}$ mice indicate altered microglial function, early therapies targeting the microglia in EPM1 should be investigated.

The investigation of physiological changes underlying the bone phenotype in EPM1 revealed altered osteoclast function and homeostasis in the form of decreased resorptive capacity due to decrease in osteoclast numbers. While we were not able to discover the why a lack of CSTB leads to the observed changes, our results demonstrated that CSTB has a role in regulating bone metabolism beyond cat K inhibition. As the function of CSTB is still poorly understood, and a possible role in regulating osteoclast homeostasis could have therapeutic implications in disorders of the bone such as osteoporosis, the role of CSTB in bone metabolism should be studied further.

Finally, the research in this thesis was also able to introduce new methods for research in mouse models of neurodegenerative diseases in the form of longitudinal TBSS. While the methodology was demonstrated here in an *ex vivo* setting, with more advanced imaging systems and shorter imaging times, *in vivo* follow-up of animal models of neurodegenerative diseases can be achieved, enabling more elegant study settings in the future.

The results shown in this thesis provided novel information about cellular and tissue level changes underlying the neuronal and bone pathologies in EPM1 and the high correlation between the mouse model and the findings in patients supplied

further affirmation for the use of the mouse model in EPM1 research. Ultimately, the results provided new insight both into the disease progression of EPM1 and the tissue level changes underlying the pathological changes present in the disease. As the background of these observed pathologies should in the future be investigated in depth, these findings raise the prospects for future research and highlight the continuity in the investigation of EPM1 pathogenesis.

6 ACKNOWLEDGEMENTS

This study was carried out at the Folkhälsan Institute of Genetics, at the Neuroscience Center and Department of Medical Genetics, University of Helsinki, and I wish to thank these instances for providing the infrastructure for my work. The late Finnish Graduate School for Neuroscience (FGSN) and as it is currently known, the Doctoral Program Brain and Mind, is also acknowledged for providing me with a fellowship. Additionally, my study was funded by the following sources: Finnish Cultural Foundation (Etelä-Savo Regional Fund), Epilepsy Research Foundation, The Finnish association of Neuroradiologists, Finnish Brain Foundation, Oskar Öflund Foundation, and Chancellor's Travel Fund of the University of Helsinki.

I would like to acknowledge prof. Päivi Peltomäki for serving as a custos for my public examination. I also wish to thank my official reviewer dos. Timo Kurki for the thorough examination of my thesis, and willingness to accept the task at such a short notice. My other reviewer prof. Heikki Tanila is thanked both for his valuable input both as a pre-examiner, and for his insightful comments while participating in my thesis advisory group. I would also like to thank the other member my thesis advisory committee, adjunct prof. Jaana Westerinen.

I'm also extremely grateful for my PhD supervisors, prof. Anna-Elina Lehesjoki and late adjunct prof. Outi Kopra, without whom I would have never started working on this project. I have to admire your enthusiasm and devotion to science. Prof. Olli Gröhn has had the role of my "third supervisor", and his input has been essential for my work. I would also like to thank all the current and former members of Olli's lab, I have always felt welcome coming to Kuopio.

The co-authors and collaborators are also thanked for valuable contribution for my PhD work. First and foremost, I'd like to thank Prof. Ritva Vanninen and Dr. Päivi Koskenkorva for their help, and patience with the submissions and revisions, and Prof Hannu Kalimo for guiding me into the field of electron microscopy. Furthermore, Teemu Laitinen and Kimmo Lehtimäki deserve to recognized for instructing me in the use of TBSS. I also would like to thank the prof. Riku Kiviranta, and Dr. Tiina Laitala-Leinonen and their respective labs for helping me finalize my last paper.

Additionally, I wish to thank all the current and former Folkhälsan Research center people, especially Vilma, Anna, Jaakko, Hanna, Naula, Ann-Liz, Kaisa, Anne, Maria, and pH. And foremost to the AEL-research group, I must present my warmest thanks, you are a lovely bunch of people to work with. Most importantly Paula, you keeping the lab running and have always helped me with practical things, without you, I would have never found anything in the lab and would forever roam the lab looking for antibodies. Saara, and Mervi, you were always the ones that I would bother with

my questions, and seeing you graduate was a light at the end of the tunnel for me. I always have had a blast travelling with you, and it hasn't been quite the same since you two left. My thanks also to Tarja, for being the expert to talk to when Outi or Anna-Elina could not be located. Anni, thanks for being my support person in the lab, you're going to be missed. Inken, thanks for being so sensible and organized, seeing you doing and planning your experiments is always such a joy. Edu and Mikko, it's up to you to be the men in the group, and Olesya and Kata keep up the good work.

To my dear friends, relatives and acquaintances, I would like to give my biggest thanks, for providing me with a life outside of work. And to my family, my parents and my sister, I owe my deepest gratitude for continuously supporting me while I was working on my thesis.

And last, Krisse, thank you for being there for me.

Helsinki, Septemper 2015

7 REFERENCES

Akman, C.I., Provenzano, F., Wang, D., Engelstad, K., Hinton, V., Yu, J., Tikofsky, R., Ichese, M. & De Vivo, D.C. 2015, "Topography of brain glucose hypometabolism and epileptic network in glucose transporter 1 deficiency", *Epilepsy research,* vol. 110, pp. 206-215.

Allen, N.J. & Barres, B.A. 2009, "Neuroscience: Glia - more than just brain glue", *Nature,* vol. 457, no. 7230, pp. 675-677.

Bagshaw, A.P., Rollings, D.T., Khalsa, S. & Cavanna, A.E. 2014, "Multimodal neuroimaging investigations of alterations to consciousness: the relationship between absence epilepsy and sleep", *Epilepsy & behavior : E&B,* vol. 30, pp. 33-37.

Baumann, N. & Pham-Dinh, D. 2001, "Biology of oligodendrocyte and myelin in the mammalian central nervous system", *Physiological Reviews,* vol. 81, no. 2, pp. 871-927.

Begonia, M.T., Prabhu, R., Liao, J., Whittington, W.R., Claude, A., Willeford, B., Wardlaw, J., Wu, R., Zhang, S. & Williams, L.N. 2014, "Quantitative analysis of brain microstructure following mild blunt and blast trauma", *Journal of Biomechanics,* vol. 47, no. 15, pp. 3704-3711.

Bellen, H.J., Tong, C. & Tsuda, H. 2010, "100 years of Drosophila research and its impact on vertebrate neuroscience: a history lesson for the future", *Nature reviews.Neuroscience,* vol. 11, no. 7, pp. 514-522.

Berg, A.T., Berkovic, S.F., Brodie, M.J., Buchhalter, J., Cross, J.H., van Emde Boas, W., Engel, J., French, J., Glauser, T.A., Mathern, G.W., Moshe, S.L., Nordli, D., Plouin, P. & Scheffer, I.E. 2010, "Revised terminology and concepts for organization of seizures and epilepsies: report of the ILAE Commission on Classification and Terminology, 2005-2009", *Epilepsia,* vol. 51, no. 4, pp. 676-685.

Berkovic, S.F., So, N.K. & Andermann, F. 1991, "Progressive myoclonus epilepsies: clinical and neurophysiological diagnosis", *Journal of clinical neurophysiology : official publication of the American Electroencephalographic Society,* vol. 8, no. 3, pp. 261-274.

Boyce, R.W., Varela, A., Chouinard, L., Bussiere, J.L., Chellman, G.J., Ominsky, M.S. & Pyrah, I.T. 2014, "Infant cynomolgus monkeys exposed to denosumab in utero exhibit an osteoclast-poor osteopetrotic-like skeletal phenotype at birth and in the early postnatal period", *Bone,* vol. 64, pp. 314-325.

Bromme, D., Rinne, R. & Kirschke, H. 1991, "Tight-binding inhibition of cathepsin S by cystatins", *Biomedica biochimica acta,* vol. 50, no. 4-6, pp. 631-635.

Buijink, A.W., Broersma, M., van der Stouwe, A.M., van Wingen, G.A., Groot, P.F., Speelman, J.D., Maurits, N.M. & van Rootselaar, A.F. 2015, "Rhythmic finger tapping reveals cerebellar dysfunction in essential tremor", *Parkinsonism & related disorders,* .

Burzynska, A.Z., Preuschhof, C., Backman, L., Nyberg, L., Li, S.C., Lindenberger, U. & Heekeren, H.R. 2010, "Age-related differences in white matter microstructure: region-specific patterns of diffusivity", *NeuroImage,* vol. 49, no. 3, pp. 2104-2112.

Butts, T., Green, M.J. & Wingate, R.J. 2014, "Development of the cerebellum: simple steps to make a 'little brain'", *Development (Cambridge, England),* vol. 141, no. 21, pp. 4031-4041.

Buzzi, A., Chikhladze, M., Falcicchia, C., Paradiso, B., Lanza, G., Soukupova, M., Marti, M., Morari, M., Franceschetti, S. & Simonato, M. 2012, "Loss of cortical GABA terminals in Unverricht-Lundborg disease", *Neurobiology of disease,* vol. 47, no. 2, pp. 216-224.

Campos, B.M., Coan, A.C., Beltramini, G.C., Liu, M., Yassuda, C.L., Ghizoni, E., Beaulieu, C., Gross, D.W. & Cendes, F. 2015, "White matter abnormalities associate with type and localization of focal epileptogenic lesions", *Epilepsia,* vol. 56, no. 1, pp. 125-132.

Caputo, N.D., Stahmer, C., Lim, G. & Shah, K. 2014, "Whole-body computed tomographic scanning leads to better survival as opposed to selective scanning in trauma patients: a systematic review and meta-analysis", *The journal of trauma and acute care surgery,* vol. 77, no. 4, pp. 534-539.

Castillo, M. 2014, "History and evolution of brain tumor imaging: insights through radiology", *Radiology,* vol. 273.

Cervinka, T., Rittweger, J., Hyttinen, J., Felsenberg, D. & Sievanen, H. 2011, "Anatomical sector analysis of load-bearing tibial bone structure during 90-day bed rest and 1-year recovery", *Clinical physiology and functional imaging,* vol. 31, no. 4, pp. 249-257.

Chahboune, H., Ment, L.R., Stewart, W.B., Ma, X., Rothman, D.L. & Hyder, F. 2007, "Neurodevelopment of C57B/L6 mouse brain assessed by in vivo diffusion tensor imaging", *NMR in biomedicine,* vol. 20, no. 3, pp. 375-382.

Chen, W., Yang, S., Abe, Y., Li, M., Wang, Y., Shao, J., Li, E. & Li, Y.P. 2007, "Novel pycnodysostosis mouse model uncovers cathepsin K function as a potential regulator of osteoclast apoptosis and senescence", *Human molecular genetics,* vol. 16, no. 4, pp. 410-423.

Chomiak, T. & Hu, B. 2009, "What is the optimal value of the g-ratio for myelinated fibers in the rat CNS? A theoretical approach", *PloS one,* vol. 4, no. 11.

Clay, H. & Coughlin, S.R. 2015, "Mechanical vessel injury in zebrafish embryos", *Journal of visualized experiments : JoVE,* vol. (96).

Coenen, V.A., Allert, N., Paus, S., Kronenburger, M., Urbach, H. & Madler, B. 2014, "Modulation of the cerebello-thalamo-cortical network in thalamic deep brain stimulation for tremor: a diffusion tensor imaging study", *Neurosurgery,* vol. 75, no. 6, pp. 657-69; discussion 669-70.

Cohen, N.R., Hammans, S.R., Macpherson, J. & Nicoll, J.A. 2011, "New neuropathological findings in Unverricht-Lundborg disease: neuronal intranuclear and cytoplasmic inclusions", *Acta Neuropathologica,* vol. 121, no. 3, pp. 421-427.

Concha, L., Gross, D.W., Wheatley, B.M. & Beaulieu, C. 2006, "Diffusion tensor imaging of time-dependent axonal and myelin degradation after corpus callosotomy in epilepsy patients", *NeuroImage,* vol. 32, no. 3, pp. 1090-1099.

Cosottini, M., Giannelli, M., Siciliano, G., Lazzarotti, G., Michelassi, M.C., Del Corona, A., Bartolozzi, C. & Murri, L. 2005, "Diffusion-tensor MR imaging of corticospinal tract in amyotrophic lateral sclerosis and progressive muscular atrophy", *Radiology,* vol. 237, no. 1, pp. 258-264.

Cowan, W.M., Harter, D.H. & Kandel, E.R. 2000, "The emergence of modern neuroscience: some implications for neurology and psychiatry", *Annual Review of Neuroscience,* vol. 23, pp. 343-391.

Criste, G., Trapp, B. & Dutta, R. 2014, "Axonal loss in multiple sclerosis: causes and mechanisms", *Handbook of clinical neurology,* vol. 122, pp. 101-113.

Currey, J.D. 2013, *Bones : Structure and Mechanics,* Princeton University Press, Princeton, NJ, USA.

Dacosta-Aguayo, R., Grana, M., Fernandez-Andujar, M., Lopez-Cancio, E., Caceres, C., Bargallo, N., Barrios, M., Clemente, I., Monserrat, P.T., Sas, M.A., Davalos, A., Auer, T. & Mataro, M. 2014, "Structural integrity of the contralesional hemisphere predicts cognitive impairment in ischemic stroke at three months", *PloS one,* vol. 9, no. 1.

D'Amato, E., Kokaia, Z., Nanobashvili, A., Reeben, M., Lehesjoki, A.E., Saarma, M. & Lindvall, O. 2000, "Seizures induce widespread upregulation of cystatin B, the gene mutated in progressive myoclonus epilepsy, in rat forebrain neurons", *The European journal of neuroscience,* vol. 12, no. 5, pp. 1687-1695.

Damoiseaux, J.S., Smith, S.M., Witter, M.P., Sanz-Arigita, E.J., Barkhof, F., Scheltens, P., Stam, C.J., Zarei, M. & Rombouts, S.A. 2009, "White matter tract integrity in aging and Alzheimer's disease", *Human brain mapping,* vol. 30, no. 4, pp. 1051-1059.

Danner, N., Julkunen, P., Hypponen, J., Niskanen, E., Saisanen, L., Kononen, M., Koskenkorva, P., Vanninen, R., Kalviainen, R. & Mervaala, E. 2013, "Alterations of motor cortical excitability and anatomy in Unverricht-Lundborg disease", *Movement disorders : official journal of the Movement Disorder Society,* vol. 28, no. 13, pp. 1860-1867.

Danner, N., Julkunen, P., Khyuppenen, J., Hukkanen, T., Kononen, M., Saisanen, L., Koskenkorva, P., Vanninen, R., Lehesjoki, A.E., Kalviainen, R. & Mervaala, E. 2009, "Altered cortical inhibition in Unverricht-Lundborg type progressive myoclonus epilepsy (EPM1)", *Epilepsy research,* vol. 85, no. 1, pp. 81-88.

de Haan, G.J., Halley, D.J., Doelman, J.C., Geesink, H.H., Augustijn, P.B., Jager-Jongkind, A.D., Majoie, M., Bader, A.J., Leliefeld-Ten Doeschate, L.A., Deelen, W.H., Bertram, E., Lehesjoki, A.E. & Lindhout, D. 2004, "Univerricht-Lundborg disease: underdiagnosed in the Netherlands", *Epilepsia,* vol. 45, no. 9, pp. 1061-1063.

Drijkoningen, D., Caeyenberghs, K., Leunissen, I., Vander Linden, C., Sunaert, S., Duysens, J. & Swinnen, S.P. 2014, "Training-induced improvements in postural control are accompanied by alterations in cerebellar white matter in brain injured patients", *NeuroImage.Clinical,* vol. 7, pp. 240-251.

Eldridge, R., Iivanainen, M., Stern, R., Koerber, T. & Wilder, B.J. 1983, ""Baltic" myoclonus epilepsy: hereditary disorder of childhood made worse by phenytoin", *Lancet,* vol. 2, no. 8354, pp. 838-842.

Fine, E.J., Ionita, C.C. & Lohr, L. 2002, "The history of the development of the cerebellar examination", *Seminars in neurology,* vol. 22, no. 4, pp. 375-384.

Fisher, S.E. & Marcus, G.F. 2006, "The eloquent ape: genes, brains and the evolution of language", *Nature reviews.Genetics,* vol. 7, no. 1, pp. 9-20.

Focke, N.K., Diederich, C., Helms, G., Nitsche, M.A., Lerche, H. & Paulus, W. 2014, "Idiopathic-generalized epilepsy shows profound white matter diffusion-tensor imaging alterations", *Human brain mapping,* vol. 35, no. 7, pp. 3332-3342.

Focke, N.K., Yogarajah, M., Bonelli, S.B., Bartlett, P.A., Symms, M.R. & Duncan, J.S. 2008, "Voxel-based diffusion tensor imaging in patients with mesial temporal lobe epilepsy and hippocampal sclerosis", *NeuroImage,* vol. 40, no. 2, pp. 728-737.

Franceschetti, S., Sancini, G., Buzzi, A., Zucchini, S., Paradiso, B., Magnaghi, G., Frassoni, C., Chikhladze, M., Avanzini, G. & Simonato, M. 2007, "A pathogenetic hypothesis of Unverricht-Lundborg disease onset and progression", *Neurobiology of disease,* vol. 25, no. 3, pp. 675-685.

Franklin, K.B.J. & Paxinos, G. 1997, *The mouse brain in stereotaxic coordinates,* Academic Press, San Diego.

From Nobel Lectures, Physics 1901-1921, Elsevier Publishing Company, Amsterdam, 1967 , *The Nobel Prize in Physics 1901* Available: http://nobelprize.org/nobel_prizes/physics/laureates/1901/rontgen-bio.html February 2015.

From Nobel Lectures, Physiology or Medicine 1901-1921, Elsevier Publishing Company, Amsterdam, 1967 , *The Nobel Prize in Physiology or Medicine 1906*. Available: http://www.nobelprize.org/nobel_prizes/medicine/laureates/1906/cajal-bio.html February 2015.

Fuller, K., Bayley, K.E. & Chambers, T.J. 2000, "Activin A is an essential cofactor for osteoclast induction", *Biochemical and biophysical research communications,* vol. 268, no. 1, pp. 2-7.

Gadian, D. (ed) 1995, *NRM and its applications to living systems.*, 2nd edn, Oxford University Press, Oxford.

Gelinas, J.N., Fitzpatrick, K.P., Kim, H.C. & Bjornson, B.H. 2014, "Cerebellar language mapping and cerebral language dominance in pediatric epilepsy surgery patients", *NeuroImage.Clinical,* vol. 6, pp. 296-306.

Ghai, S. & Trachtenberg, J. 2015, "In-bore MRI interventions: current status and future applications", *Current opinion in urology,* .

Green, G.D., Kembhavi, A.A., Davies, M.E. & Barrett, A.J. 1984, "Cystatin-like cysteine proteinase inhibitors from human liver", *The Biochemical journal,* vol. 218, no. 3, pp. 939-946.

Groeschel, S., i Dali, C., Clas, P., Bohringer, J., Duno, M., Krarup, C., Kehrer, C., Wilke, M. & Krageloh-Mann, I. 2012, "Cerebral gray and white matter changes and clinical course in metachromatic leukodystrophy", *Neurology,* vol. 79, no. 16, pp. 1662-1670.

Halleen, J.M., Hentunen, T.A., Karp, M., Kakonen, S.M., Pettersson, K. & Vaananen, H.K. 1998, "Characterization of serum tartrate-resistant acid phosphatase and development of a direct two-site immunoassay", *Journal of bone and mineral research : the official journal of the American Society for Bone and Mineral Research,* vol. 13, no. 4, pp. 683-687.

Haltia, M., Kristensson, K. & Sourander, P. 1969, "Neuropathological studies in three Scandinavian cases of progressive myoclonus epilepsy", *Acta Neurologica Scandinavica,* vol. 45, no. 1, pp. 63-77.

Harper, A. 2010, "Mouse models of neurological disorders--a comparison of heritable and acquired traits", *Biochimica et biophysica acta,* vol. 1802, no. 10, pp. 785-795.

Harward, S.C. & McNamara, J.O. 2014, "Aligning animal models with clinical epilepsy: where to begin?", *Advances in Experimental Medicine and Biology,* vol. 813, pp. 243-251.

Hattingen, E., Luckerath, C., Pellikan, S., Vronski, D., Roth, C., Knake, S., Kieslich, M. & Pilatus, U. 2014, "Frontal and thalamic changes of GABA concentration indicate dysfunction of thalamofrontal networks in juvenile myoclonic epilepsy", *Epilepsia,* vol. 55, no. 7, pp. 1030-1037.

Haydel, M.J., Preston, C.A., Mills, T.J., Luber, S., Blaudeau, E. & DeBlieux, P.M. 2000, "Indications for computed tomography in patients with minor head injury", *The New England journal of medicine,* vol. 343, no. 2, pp. 100-105.

Holthausen, H., Pieper, T. & Kudernatsch, M. 2013, "Towards early diagnosis and treatment to save children from catastrophic epilepsy -- focus on epilepsy surgery", *Brain & development,* vol. 35, no. 8, pp. 730-741.

Hooke, R. 1665,"Micrographia: or, Some physiological descriptions of minute bodies made by magnifying glasses. With observations and inquiries thereupon", Printed by J. Martyn and J. Allestry, London.

Houseweart, M.K., Pennacchio, L.A., Vilaythong, A., Peters, C., Noebels, J.L. & Myers, R.M. 2003, "Cathepsin B but not cathepsins L or S contributes to the pathogenesis of Unverricht-Lundborg progressive myoclonus epilepsy (EPM1)", *Journal of neurobiology,* vol. 56, no. 4, pp. 315-327.

Ibarretxe-Bilbao, N., Junque, C., Marti, M.J., Valldeoriola, F., Vendrell, P., Bargallo, N., Zarei, M. & Tolosa, E. 2010, "Olfactory impairment in Parkinson's disease and white matter abnormalities in central olfactory areas: A voxel-based diffusion tensor imaging study", *Movement disorders : official journal of the Movement Disorder Society,* vol. 25, no. 12, pp. 1888-1894.

Itoh, K., Udagawa, N., Katagiri, T., Iemura, S., Ueno, N., Yasuda, H., Higashio, K., Quinn, J.M., Gillespie, M.T., Martin, T.J., Suda, T. & Takahashi, N. 2001, "Bone morphogenetic protein 2 stimulates osteoclast differentiation and survival supported by receptor activator of nuclear factor-kappaB ligand", *Endocrinology,* vol. 142, no. 8, pp. 3656-3662.

Jenkinson, M., Bannister, P., Brady, M. & Smith, S. 2002, "Improved optimization for the robust and accurate linear registration and motion correction of brain images", *NeuroImage,* vol. 17, no. 2, pp. 825-841.

Jenkinson, M. & Smith, S. 2001, "A global optimisation method for robust affine registration of brain images", *Medical image analysis,* vol. 5, no. 2, pp. 143-156.

Joensuu, T., Lehesjoki, A.E. & Kopra, O. 2008, "Molecular background of EPM1-Unverricht-Lundborg disease", *Epilepsia,* vol. 49, no. 4, pp. 557-563.

Joensuu, T., Tegelberg, S., Reinmaa, E., Segerstrale, M., Hakala, P., Pehkonen, H., Korpi, E.R., Tyynela, J., Taira, T., Hovatta, I., Kopra, O. & Lehesjoki, A.E. 2014, "Gene expression alterations in the cerebellum and granule neurons of Cstb(-/-) mouse are associated with early synaptic changes and inflammation", *PloS one,* vol. 9, no. 2.

Kälviäinen, R., Khyuppenen, J., Koskenkorva, P., Eriksson, K., Vanninen, R. & Mervaala, E. 2008, "Clinical picture of EPM1-Unverricht-Lundborg disease", *Epilepsia,* vol. 49, no. 4, pp. 549-556.

Kattan, K.R. 1970, "Calvarial thickening after Dilantin medication", *The American Journal of Roentgenology, Radium Therapy, and Nuclear Medicine,* vol. 110, no. 1, pp. 102-105.

Kim, J.B., Suh, S.I., Seo, W.K., Oh, K., Koh, S.B. & Kim, J.H. 2014, "Altered thalamocortical functional connectivity in idiopathic generalized epilepsy", *Epilepsia,* vol. 55, no. 4, pp. 592-600.

Kiviranta, R., Morko, J., Alatalo, S.L., NicAmhlaoibh, R., Risteli, J., Laitala-Leinonen, T. & Vuorio, E. 2005, "Impaired bone resorption in cathepsin K-deficient mice is partially compensated for by enhanced osteoclastogenesis and increased expression of other proteases via an increased RANKL/OPG ratio", *Bone,* vol. 36, no. 1, pp. 159-172.

Kominami, E., Bando, Y., Wakamatsu, N. & Katunuma, N. 1984, "Different tissue distributions of two types of thiol proteinase inhibitors from rat liver and epidermis", *Journal of Biochemistry,* vol. 96, no. 5, pp. 1437-1442.

Korbekandi, H., Chitsazi, M.R., Asghari, G., Bahri Najafi, R., Badii, A. & Iravani, S. 2015, "Green biosynthesis of silver nanoparticles using Quercus brantii (oak) leaves hydroalcoholic extract", *Pharmaceutical Biology,* , pp. 1-6.

Korja, M., Kaasinen, V., Lamusuo, S., Marttila, R.J. & Parkkola, R. 2007a, "Hyperostosis frontalis interna as a novel finding in Unverricht-Lundborg disease", *Neurology,* vol. 68, no. 13, pp. 1077-1078.

Korja, M., Kaasinen, V., Lamusuo, S., Parkkola, R., Nagren, K. & Marttila, R.J. 2007b, "Substantial thalamostriatal dopaminergic defect in Unverricht-Lundborg disease", *Epilepsia,* vol. 48, no. 9, pp. 1768-1773.

Koskenkorva, P., Hypponen, J., Aikia, M., Mervaala, E., Kiviranta, T., Eriksson, K., Lehesjoki, A.E., Vanninen, R. & Kalviainen, R. 2011, "Severer phenotype in Unverricht-Lundborg disease (EPM1) patients compound heterozygous for the dodecamer repeat expansion and the c.202C>T mutation in the CSTB gene", *Neuro-degenerative diseases,* vol. 8, no. 6, pp. 515-522.

Koskenkorva, P., Khyuppenen, J., Niskanen, E., Kononen, M., Bendel, P., Mervaala, E., Lehesjoki, A.E., Kalviainen, R. & Vanninen, R. 2009, "Motor cortex and thalamic atrophy in Unverricht-Lundborg disease: voxel-based morphometric study", *Neurology,* vol. 73, no. 8, pp. 606-611.

Koskenkorva, P., Niskanen, E., Hypponen, J., Kononen, M., Mervaala, E., Soininen, H., Kalviainen, R. & Vanninen, R. 2012, "Sensorimotor, visual, and auditory cortical atrophy in Unverricht-Lundborg disease mapped with cortical thickness analysis", *AJNR.American journal of neuroradiology,* vol. 33, no. 5, pp. 878-883.

Koskiniemi, M., Donner, M., Majuri, H., Haltia, M. & Norio, R. 1974, "Progressive myoclonus epilepsy. A clinical and histopathological study", *Acta Neurologica Scandinavica,* vol. 50, no. 3, pp. 307-332.

Kuronen, M., Hermansson, M., Manninen, O., Zech, I., Talvitie, M., Laitinen, T., Grohn, O., Somerharju, P., Eckhardt, M., Cooper, J.D., Lehesjoki, A.E., Lahtinen, U. & Kopra, O. 2012, "Galactolipid deficiency in the early pathogenesis of neuronal ceroid lipofuscinosis model Cln8mnd : implications to delayed myelination and oligodendrocyte maturation", *Neuropathology and applied neurobiology,* vol. 38, no. 5, pp. 471-486.

Laitala-Leinonen, T., Rinne, R., Saukko, P., Vaananen, H.K. & Rinne, A. 2006, "Cystatin B as an intracellular modulator of bone resorption", *Matrix biology : journal of the International Society for Matrix Biology,* vol. 25, no. 3, pp. 149-157.

Lalioti, M.D., Mirotsou, M., Buresi, C., Peitsch, M.C., Rossier, C., Ouazzani, R., Baldy-Moulinier, M., Bottani, A., Malafosse, A. & Antonarakis, S.E. 1997, "Identification of mutations in cystatin B, the gene responsible for the Unverricht-Lundborg type of progressive myoclonus epilepsy (EPM1)", *American Journal of Human Genetics,* vol. 60, no. 2, pp. 342-351.

Larvaron, P., Boespflug-Tanguy, O., Renou, J.P. & Bonny, J.M. 2007, "In vivo analysis of the post-natal development of normal mouse brain by DTI", *NMR in biomedicine,* vol. 20, no. 4, pp. 413-421.

Lau, J.C., Lerch, J.P., Sled, J.G., Henkelman, R.M., Evans, A.C. & Bedell, B.J. 2008, "Longitudinal neuroanatomical changes determined by deformation-based morphometry in a mouse model of Alzheimer's disease", *NeuroImage,* vol. 42, no. 1, pp. 19-27.

Lehtinen, M.K., Tegelberg, S., Schipper, H., Su, H., Zukor, H., Manninen, O., Kopra, O., Joensuu, T., Hakala, P., Bonni, A. & Lehesjoki, A.E. 2009, "Cystatin B deficiency sensitizes neurons to oxidative stress in progressive myoclonus epilepsy, EPM1", *The Journal of neuroscience : the official journal of the Society for Neuroscience,* vol. 29, no. 18, pp. 5910-5915.

Li, X., Westman, E., Stahlbom, A.K., Thordardottir, S., Almkvist, O., Blennow, K., Wahlund, L.O. & Graff, C. 2015, "White matter changes in familial Alzheimer's disease", *Journal of internal medicine,* .

Lieuallen, K., Pennacchio, L.A., Park, M., Myers, R.M. & Lennon, G.G. 2001, "Cystatin B-deficient mice have increased expression of apoptosis and glial activation genes", *Human molecular genetics,* vol. 10, no. 18, pp. 1867-1871.

Liu, Y., Spulber, G., Lehtimaki, K.K., Kononen, M., Hallikainen, I., Grohn, H., Kivipelto, M., Hallikainen, M., Vanninen, R. & Soininen, H. 2011, "Diffusion tensor imaging and tract-based spatial statistics in Alzheimer's disease and mild cognitive impairment", *Neurobiology of aging,* vol. 32, no. 9, pp. 1558-1571.

Liu, Z., Zhang, X., Yu, Q. & He, J.J. 2014, "Exosome-associated hepatitis C virus in cell cultures and patient plasma", *Biochemical and biophysical research communications,* vol. 455, no. 3-4, pp. 218-222.

Llinas, R.R. 2003, "The contribution of Santiago Ramon y Cajal to functional neuroscience", *Nature reviews.Neuroscience,* vol. 4, no. 1, pp. 77-80.

Lundborg, H. 1912, "Der Erbgang der progressiven Myoklonus-Epilepsie. (Myoklonie-Epilepsie s. Unverrichts familiäre Myoklonie)", vol. 9, no. 1.

Lundborg, H. 1903, *Die progressive Myoklonus Epilepsie,* , Upsala.

Ma, J., Tanaka, K.F., Yamada, G. & Ikenaka, K. 2007, "Induced expression of cathepsins and cystatin C in a murine model of demyelination", *Neurochemical research,* vol. 32, no. 2, pp. 311-320.

Madhyastha, T., Merillat, S., Hirsiger, S., Bezzola, L., Liem, F., Grabowski, T. & Jancke, L. 2014, "Longitudinal reliability of tract-based spatial statistics in diffusion tensor imaging", *Human brain mapping,* vol. 35, no. 9, pp. 4544-4555.

Magaudda, A., Ferlazzo, E., Nguyen, V.H. & Genton, P. 2006, "Unverricht-Lundborg disease, a condition with self-limited progression: long-term follow-up of 20 patients", *Epilepsia,* vol. 47, no. 5, pp. 860-866.

Malafosse, A., Lehesjoki, A.E., Genton, P., Labauge, P., Durand, G., Tassinari, C.A., Dravet, C., Michelucci, R. & de la Chapelle, A. 1992, "Identical genetic locus for Baltic and Mediterranean myoclonus", *Lancet,* vol. 339, no. 8801, pp. 1080-1081.

Mallucci, G., Peruzzotti-Jametti, L., Bernstock, J.D. & Pluchino, S. 2015, "The role of immune cells, glia and neurons in white and gray matter pathology in multiple sclerosis", *Progress in neurobiology.*

Manto, M., Bower, J.M., Conforto, A.B., Delgado-Garcia, J.M., da Guarda, S.N., Gerwig, M., Habas, C., Hagura, N., Ivry, R.B., Marien, P., Molinari, M., Naito, E., Nowak, D.A., Oulad Ben Taib, N., Pelisson, D., Tesche, C.D., Tilikete, C. & Timmann, D. 2012, "Consensus paper: roles of the cerebellum in motor control--the diversity of ideas on cerebellar involvement in movement", *Cerebellum,* vol. 11, no. 2, pp. 457-487.

Marien, P., Ackermann, H., Adamaszek, M., Barwood, C.H., Beaton, A., Desmond, J., De Witte, E., Fawcett, A.J., Hertrich, I., Kuper, M., Leggio, M., Marvel, C., Molinari, M., Murdoch, B.E., Nicolson, R.I., Schmahmann, J.D., Stoodley, C.J., Thurling, M., Timmann, D., Wouters, E. & Ziegler, W. 2014, "Consensus paper: Language and the cerebellum: an ongoing enigma", *Cerebellum,* vol. 13, no. 3, pp. 386-410.

Mascalchi, M., Diciotti, S., Giannelli, M., Ginestroni, A., Soricelli, A., Nicolai, E., Aiello, M., Tessa, C., Galli, L., Dotti, M.T., Piacentini, S., Salvatore, E. & Toschi, N. 2014, "Progression of brain atrophy in spinocerebellar ataxia type 2: a longitudinal tensor-based morphometry study", *PloS one,* vol. 9, no. 2.

Mascalchi, M., Michelucci, R., Cosottini, M., Tessa, C., Lolli, F., Riguzzi, P., Lehesjoki, A.E., Tosetti, M., Villari, N. & Tassinari, C.A. 2002, "Brainstem involvement in Unverricht-Lundborg disease (EPM1): An MRI and (1)H MRS study", *Neurology,* vol. 58, no. 11, pp. 1686-1689.

McGowan, H.W., Schuijers, J.A., Grills, B.L., McDonald, S.J. & McDonald, A.C. 2014, "Galnon, a galanin receptor agonist, improves intrinsic cortical bone tissue properties but exacerbates bone loss in an ovariectomised rat model", *Journal of Musculoskeletal & Neuronal Interactions,* vol. 14, no. 2, pp. 162-172.

Melo, T.P., Bogousslavsky, J., Moulin, T., Nader, J. & Regli, F. 1992, "Thalamic ataxia", *Journal of neurology,* vol. 239, no. 6, pp. 331-337.

Meng, Y., Payne, C., Li, L., Hu, X., Zhang, X. & Bachevalier, J. 2014, "Alterations of hippocampal projections in adult macaques with neonatal hippocampal lesions: a Diffusion Tensor Imaging study", *NeuroImage,* vol. 102 Pt 2, pp. 828-837.

Mervaala, E., Keranen, T., Paakkonen, A., Partanen, J.V. & Riekkinen, P. 1986, "Visual evoked potentials, brainstem auditory evoked potentials, and quantitative EEG in Baltic progressive myoclonus epilepsy", *Epilepsia,* vol. 27, no. 5, pp. 542-547.

Mervaala, E., Partanen, J.V., Keranen, T., Penttila, M. & Riekkinen, P. 1984, "Prolonged cortical somatosensory evoked potential latencies in progressive myoclonus epilepsy", *Journal of the neurological sciences,* vol. 64, no. 2, pp. 131-135.

Minassian, B.A. 2014, "The progressive myoclonus epilepsies", *Progress in brain research,* vol. 213, pp. 113-122.

Mori, S. 2007, *Introduction to diffusion tensor imaging,* Elsevier, Amsterdam ; Oxford.

Morin, N., Jourdain, V.A. & Di Paolo, T. 2014, "Modeling dyskinesia in animal models of Parkinson disease", *Experimental neurology,* vol. 256, pp. 105-116.

Morrissette, D.A., Parachikova, A., Green, K.N. & LaFerla, F.M. 2009, "Relevance of transgenic mouse models to human Alzheimer disease", *The Journal of biological chemistry,* vol. 284, no. 10, pp. 6033-6037.

Nguyen, D. & Xu, T. 2008, "The expanding role of mouse genetics for understanding human biology and disease", *Disease models & mechanisms,* vol. 1, no. 1, pp. 56-66.

Niskanen, J. , *Aedes – A graphical tool for analyzing medical images*. Available: http://aedes.uef.fi/ [2015, February].

Noebels, J. 2015, "Pathway-driven discovery of epilepsy genes", *Nature neuroscience,* vol. 18, no. 3, pp. 344-350.

Norio, R. 2003, "Finnish Disease Heritage I: characteristics, causes, background", *Human genetics,* vol. 112, no. 5-6, pp. 441-456.

Norio, R. & Koskiniemi, M. 1979, "Progressive myoclonus epilepsy: genetic and nosological aspects with special reference to 107 Finnish patients", *Clinical genetics,* vol. 15, no. 5, pp. 382-398.

Nurmio, M., Joki, H., Kallio, J., Maatta, J.A., Vaananen, H.K., Toppari, J., Jahnukainen, K. & Laitala-Leinonen, T. 2011, "Receptor tyrosine kinase inhibition causes simultaneous bone loss and excess bone formation within growing bone in rats", *Toxicology and applied pharmacology,* vol. 254, no. 3, pp. 267-279.

Okamoto, M., Murai, J., Yoshikawa, H. & Tsumaki, N. 2006, "Bone morphogenetic proteins in bone stimulate osteoclasts and osteoblasts during bone development", *Journal of bone and mineral research : the official journal of the American Society for Bone and Mineral Research,* vol. 21, no. 7, pp. 1022-1033.

Okuneva, O., Korber, I., Li, Z., Tian, L., Joensuu, T., Kopra, O. & Lehesjoki, A.E. 2015, "Abnormal microglial activation in the Cstb(-/-) mouse, a model for progressive myoclonus epilepsy, EPM1", *Glia,* vol. 63, no. 3, pp. 400-411.

Ortega, N., Behonick, D., Stickens, D. & Werb, Z. 2003, "How proteases regulate bone morphogenesis", *Annals of the New York Academy of Sciences,* vol. 995, pp. 109-116.

Pennacchio, L.A., Bouley, D.M., Higgins, K.M., Scott, M.P., Noebels, J.L. & Myers, R.M. 1998, "Progressive ataxia, myoclonic epilepsy and cerebellar apoptosis in cystatin B-deficient mice", *Nature genetics,* vol. 20, no. 3, pp. 251-258.

Pennacchio, L.A., Lehesjoki, A.E., Stone, N.E., Willour, V.L., Virtaneva, K., Miao, J., D'Amato, E., Ramirez, L., Faham, M., Koskiniemi, M., Warrington, J.A., Norio, R., de la Chapelle, A., Cox, D.R. & Myers, R.M. 1996, "Mutations in the gene encoding cystatin B in progressive myoclonus epilepsy (EPM1)", *Science,* vol. 271, no. 5256, pp. 1731-1734.

Pennycook, S.J. 2012, "Seeing the atoms more clearly: STEM imaging from the Crewe era to today", *Ultramicroscopy,* vol. 123, pp. 28-37.

Pinto, E., Freitas, J., Duarte, A.J., Ribeiro, I., Ribeiro, D., Lima, J.L., Chaves, J. & Amaral, O. 2012, "Unverricht-Lundborg disease: homozygosity for a new splicing mutation in the cystatin B gene", *Epilepsy research,* vol. 99, no. 1-2, pp. 187-190.

Plaisier, A., Raets, M.M., Ecury-Goossen, G.M., Govaert, P., Feijen-Roon, M., Reiss, I.K., Smit, L.S., Lequin, M.H. & Dudink, J. 2015, "Serial cranial ultrasonography or early MRI for detecting preterm brain injury?", *Archives of disease in childhood.Fetal and neonatal edition,* .

Poudel, G.R., Stout, J.C., Dominguez, D.J.F., Churchyard, A., Chua, P., Egan, G.F. & Georgiou-Karistianis, N. 2015, "Longitudinal change in white matter microstructure in Huntington's disease: The IMAGE-HD study", *Neurobiology of disease,* vol. 74, pp. 406-412.

Prinz, M. & Mildner, A. 2011, "Microglia in the CNS: immigrants from another world", *Glia,* vol. 59, no. 2, pp. 177-187.

Purves, D. 2012, *Neuroscience,* 5th edn, Sinauer Associates, Sunderland, Mass.

Ravindra, V.M., Riva-Cambrin, J., Sivakumar, W., Metzger, R.R. & Bollo, R.J. 2015, "Risk factors for traumatic blunt cerebrovascular injury diagnosed by computed tomography angiography in the pediatric population: a retrospective cohort study", *Journal of neurosurgery.Pediatrics,* , pp. 1-8.

Rinne, R., Saukko, P., Jarvinen, M. & Lehesjoki, A.E. 2002, "Reduced cystatin B activity correlates with enhanced cathepsin activity in progressive myoclonus epilepsy", *Annals of Medicine,* vol. 34, no. 5, pp. 380-385.

Ritonja, A., Machleidt, W. & Barrett, A.J. 1985, "Amino acid sequence of the intracellular cysteine proteinase inhibitor cystatin B from human liver", *Biochemical and biophysical research communications,* vol. 131, no. 3, pp. 1187-1192.

Roivainen, R., Karvonen, M.K. & Puumala, T. 2014, "Seizure control in Unverricht-Lundborg disease: a single-centre study", *Epileptic disorders : international epilepsy journal with videotape,* vol. 16, no. 2, pp. 191-195.

Ruest, T., Holmes, W.M., Barrie, J.A., Griffiths, I.R., Anderson, T.J., Dewar, D. & Edgar, J.M. 2011, "High-resolution diffusion tensor imaging of fixed brain in a mouse model of Pelizaeus-Merzbacher disease: comparison with quantitative measures of white matter pathology", *NMR in biomedicine,* vol. 24, no. 10, pp. 1369-1379.

Sailer, U., Eggert, T. & Straube, A. 2005, "Impaired temporal prediction and eye-hand coordination in patients with cerebellar lesions", *Behavioural brain research,* vol. 160, no. 1, pp. 72-87.

Sasakura, H., Tsukada, Y., Takagi, S. & Mori, I. 2013, "Japanese studies on neural circuits and behavior of Caenorhabditis elegans", *Frontiers in neural circuits,* vol. 7, pp. 187.

Schneider, C.A., Rasband, W.S. & Eliceiri, K.W. 2012, "NIH Image to ImageJ: 25 years of image analysis", *Nature methods,* vol. 9, no. 7, pp. 671-675.

Schreiber, J.J., Anderson, P.A. & Hsu, W.K. 2014, "Use of computed tomography for assessing bone mineral density", *Neurosurgical focus,* vol. 37, no. 1, pp. E4.

Semelka, R.C., Armao, D.M., Elias, J.,Jr & Huda, W. 2007, "Imaging strategies to reduce the risk of radiation in CT studies, including selective substitution with MRI", *Journal of magnetic resonance imaging : JMRI,* vol. 25, no. 5, pp. 900-909.

Sen, P.N. & Basser, P.J. 2005, "A model for diffusion in white matter in the brain", *Biophysical journal,* vol. 89, no. 5, pp. 2927-2938.

Shannon, P., Pennacchio, L.A., Houseweart, M.K., Minassian, B.A. & Myers, R.M. 2002, "Neuropathological changes in a mouse model of progressive myoclonus epilepsy: cystatin B deficiency and Unverricht-Lundborg disease", *Journal of neuropathology and experimental neurology,* vol. 61, no. 12, pp. 1085-1091.

Shorvon, S.D. 2011, "The etiologic classification of epilepsy", *Epilepsia,* vol. 52, no. 6, pp. 1052-1057.

Sidaros, A., Engberg, A.W., Sidaros, K., Liptrot, M.G., Herning, M., Petersen, P., Paulson, O.B., Jernigan, T.L. & Rostrup, E. 2008, "Diffusion tensor imaging during recovery from severe traumatic brain injury and relation to clinical outcome: a longitudinal study", *Brain : a journal of neurology,* vol. 131, no. Pt 2, pp. 559-572.

Sierra, A., Laitinen, T., Lehtimaki, K., Rieppo, L., Pitkanen, A. & Grohn, O. 2011, "Diffusion tensor MRI with tract-based spatial statistics and histology reveals undiscovered lesioned areas in kainate model of epilepsy in rat", *Brain structure & function,* vol. 216, no. 2, pp. 123-135.

Singh, H., Cooper, R.J., Wai Lee, C., Dempsey, L., Edwards, A., Brigadoi, S., Airantzis, D., Everdell, N., Michell, A., Holder, D., Hebden, J.C. & Austin, T. 2014, "Mapping cortical haemodynamics during neonatal seizures using diffuse optical tomography: a case study", *NeuroImage. Clinical,* vol. 5, pp. 256-265.

Smith, S.M., Jenkinson, M., Johansen-Berg, H., Rueckert, D., Nichols, T.E., Mackay, C.E., Watkins, K.E., Ciccarelli, O., Cader, M.Z., Matthews, P.M. & Behrens, T.E. 2006, "Tract-based spatial statistics: voxelwise analysis of multi-subject diffusion data", *NeuroImage,* vol. 31, no. 4, pp. 1487-1505.

Smith, S.M., Jenkinson, M., Woolrich, M.W., Beckmann, C.F., Behrens, T.E., Johansen-Berg, H., Bannister, P.R., De Luca, M., Drobnjak, I., Flitney, D.E., Niazy, R.K., Saunders, J., Vickers, J., Zhang, Y., De Stefano, N., Brady, J.M. & Matthews, P.M. 2004, "Advances in functional and structural MR image analysis and implementation as FSL", *NeuroImage,* vol. 23 Suppl 1, pp. S208-19.

Smith, S.M., Johansen-Berg, H., Jenkinson, M., Rueckert, D., Nichols, T.E., Miller, K.L., Robson, M.D., Jones, D.K., Klein, J.C., Bartsch, A.J. & Behrens, T.E. 2007, "Acquisition and voxelwise analysis of multi-subject diffusion data with tract-based spatial statistics", *Nature protocols,* vol. 2, no. 3, pp. 499-503.

Smith, S.M. & Nichols, T.E. 2009, "Threshold-free cluster enhancement: addressing problems of smoothing, threshold dependence and localisation in cluster inference", *NeuroImage,* vol. 44, no. 1, pp. 83-98.

Soimakallio, S., Kivisaari, L., Manninen, H., Svedström, E., Tervonen, O. & Müller, E. 2005, *Radiologia,* Wsoy, Porvoo ; Helsinki.

Solomon, D.H., Barohn, R.J., Bazan, C. & Grissom, J. 1994, "The thalamic ataxia syndrome", *Neurology,* vol. 44, no. 5, pp. 810-814.

Sommer, M.A. 2003, "The role of the thalamus in motor control", *Current opinion in neurobiology,* vol. 13, no. 6, pp. 663-670.

Strata, P. 2015, "The Emotional Cerebellum", *Cerebellum*.

Sun, S.W., Liang, H.F., Cross, A.H. & Song, S.K. 2008, "Evolving Wallerian degeneration after transient retinal ischemia in mice characterized by diffusion tensor imaging", *NeuroImage,* vol. 40, no. 1, pp. 1-10.

Suoranta, S., Holli-Helenius, K., Koskenkorva, P., Niskanen, E., Kononen, M., Aikia, M., Eskola, H., Kalviainen, R. & Vanninen, R. 2013, "3D texture analysis reveals imperceptible MRI textural alterations in the thalamus and putamen in progressive myoclonic epilepsy type 1, EPM1", *PloS one,* vol. 8, no. 7.

Suoranta, S., Manninen, H., Koskenkorva, P., Kononen, M., Laitinen, R., Lehesjoki, A.E., Kalviainen, R. & Vanninen, R. 2012, "Thickened skull, scoliosis and other skeletal findings in Unverricht-Lundborg disease link cystatin B function to bone metabolism", *Bone,* vol. 51, no. 6, pp. 1016-1024.

Tegelberg, S., Kopra, O., Joensuu, T., Cooper, J.D. & Lehesjoki, A.E. 2012, "Early microglial activation precedes neuronal loss in the brain of the Cstb-/- mouse model of progressive myoclonus epilepsy, EPM1", *Journal of neuropathology and experimental neurology,* vol. 71, no. 1, pp. 40-53.

Tu, T.W., Kim, J.H., Yin, F.Q., Jakeman, L.B. & Song, S.K. 2013, "The impact of myelination on axon sparing and locomotor function recovery in spinal cord injury assessed using diffusion tensor imaging", *NMR in biomedicine,* vol. 26, no. 11, pp. 1484-1495.

Unverricht, H. 1895, "Ueber familiaere Myoclonie", *Dtsch. Z. Nervenheilk,* , no. 7, pp. 32-67.

Unverricht, H. 1891, "Die Myoclonie", *F Deuticke. Austria,* .

Vaarmann, A., Kaasik, A. & Zharkovsky, A. 2006, "Altered tryptophan metabolism in the brain of cystatin B-deficient mice: a model system for progressive myoclonus epilepsy", *Epilepsia,* vol. 47, no. 10, pp. 1650-1654.

Verma, R., Mori, S., Shen, D., Yarowsky, P., Zhang, J. & Davatzikos, C. 2005, "Spatiotemporal maturation patterns of murine brain quantified by diffusion tensor MRI and deformation-based morphometry", *Proceedings of the National Academy of Sciences of the United States of America,* vol. 102, no. 19, pp. 6978-6983.

Vogiatzi, M.G., Tsay, J., Verdelis, K., Rivella, S., Grady, R.W., Doty, S., Giardina, P.J. & Boskey, A.L. 2010, "Changes in bone microarchitecture and biomechanical properties in the th3 thalassemia mouse are associated with decreased bone turnover and occur during the period of bone accrual", *Calcified tissue international,* vol. 86, no. 6, pp. 484-494.

Williams, D.B. & Carter, C.B. 2009, *Transmission electron microscopy: a textbook for materials science,* 2nd edn, Springer, New York.

Wilson, S.R., Peters, C., Saftig, P. & Bromme, D. 2009, "Cathepsin K activity-dependent regulation of osteoclast actin ring formation and bone resorption", *The Journal of biological chemistry,* vol. 284, no. 4, pp. 2584-2592.

Wolf, U., Rapoport, M.J. & Schweizer, T.A. 2009, "Evaluating the affective component of the cerebellar cognitive affective syndrome", *The Journal of neuropsychiatry and clinical neurosciences,* vol. 21, no. 3, pp. 245-253.

Worgall, S., Kekatpure, M.V., Heier, L., Ballon, D., Dyke, J.P., Shungu, D., Mao, X., Kosofsky, B., Kaplitt, M.G., Souweidane, M.M., Sondhi, D., Hackett, N.R., Hollmann, C. & Crystal, R.G. 2007, "Neurological deterioration in late infantile neuronal ceroid lipofuscinosis", *Neurology,* vol. 69, no. 6, pp. 521-535.

Wutzl, A., Brozek, W., Lernbass, I., Rauner, M., Hofbauer, G., Schopper, C., Watzinger, F., Peterlik, M. & Pietschmann, P. 2006, "Bone morphogenetic proteins 5 and 6 stimulate osteoclast generation", *Journal of biomedical materials research.Part A,* vol. 77, no. 1, pp. 75-83.

Xing, L., Xiu, Y. & Boyce, B.F. 2012, "Osteoclast fusion and regulation by RANKL-dependent and independent factors", *World journal of orthopedics,* vol. 3, no. 12, pp. 212-222.

Zhang, K., Wang, C., Chen, Y., Ji, X., Chen, X., Tian, L. & Yu, X. 2015, "Preservation of high-fat diet-induced femoral trabecular bone loss through genetic target of TNF-alpha", *Endocrine.*

Zimmermann, E., Ostendorf, F., Ploner, C.J. & Lappe, M. 2015, "Impairment of saccade adaptation in a patient with a focal thalamic lesion", *Journal of neurophysiology,* .